2022-06

MODELING AND SIMULATIONS FOR OPTIMIZATION OF MICROFLUIDIC MICROCAPACITOR ARRAYS OF BIOMIMETIC ARTIFICIAL MUSCLES FOR QUIET PROPULSION AND EXOSKELETAL LOCOMOTION

Keeven, Joshua M.; Leckie, Jacob M.

Monterey, CA; Naval Postgraduate School

NAVAL POSTGRADUATE SCHOOL

MONTEREY, CALIFORNIA

THESIS

MODELING AND SIMULATIONS FOR OPTIMIZATION OF MICROFLUIDIC MICROCAPACITOR ARRAYS OF BIOMIMETIC ARTIFICIAL MUSCLES FOR QUIET PROPULSION AND EXOSKELETAL LOCOMOTION

by

Joshua M. Keeven and Jacob M. Leckie

June 2022

Thesis Advisor:	Emil P. Kartalov
Co-Advisor:	Amela Sadagic
Second Reader:	Quinn Kennedy

Research for this thesis was performed at the MOVES Institute.

THIS PAGE INTENTIONALLY LEFT BLANK

REPORT DOCUMENTATION PAGE			*Form Approved OMB No. 0704-0188*

1. AGENCY USE ONLY *(Leave blank)*	**2. REPORT DATE** June 2022	**3. REPORT TYPE AND DATES COVERED** Master's thesis

4. TITLE AND SUBTITLE
MODELING AND SIMULATIONS FOR OPTIMIZATION OF MICROFLUIDIC MICROCAPACITOR ARRAYS OF BIOMIMETIC ARTIFICIAL MUSCLES FOR QUIET PROPULSION AND EXOSKELETAL LOCOMOTION

5. FUNDING NUMBERS

6. AUTHOR(S) Joshua M. Keeven and Jacob M. Leckie

7. PERFORMING ORGANIZATION NAME(S) AND ADDRESS(ES)
Naval Postgraduate School
Monterey, CA 93943-5000

8. PERFORMING ORGANIZATION REPORT NUMBER

9. SPONSORING / MONITORING AGENCY NAME(S) AND ADDRESS(ES)
N/A

10. SPONSORING / MONITORING AGENCY REPORT NUMBER

11. SUPPLEMENTARY NOTES The views expressed in this thesis are those of the author and do not reflect the official policy or position of the Department of Defense or the U.S. Government.

12a. DISTRIBUTION / AVAILABILITY STATEMENT
Approved for public release. Distribution is unlimited.

12b. DISTRIBUTION CODE
A

13. ABSTRACT (maximum 200 words)

The technology that we focused on was the biomimetic actuation of microfluidic microcapacitors, which are electrostatically actuated structures that contract and function like biological muscles. Our thesis aims to find the optimal muscle-to-tendon ratio while expanding both the standard and gap design arrays and to find the respective force-density saturation values so predicted force output can be calculated for muscle fibers of a practical size. We also studied if a 3D virtual object can be a suitable model for the human operators' examination of the artificial muscle and the optimization of its structure. Our results showed a maximum force density saturation of 8800 Pa and 6700 Pa when simulating the standard and gap array respectively with planar polarity wired artificial muscles. The optimal muscle-to-tendon ratio from the data gathered on the standard array simulations is approximately 9 to 1, meaning 90 percent of the surface area of the XY plane represents microfluidic capacitors and 10 percent is dielectric tendon material. The optimal muscle to tendon ratio from the data gathered on the gap array simulations is approximately 75 to 25, meaning 75 percent of the surface area of the XY plane are microfluidic capacitors, and 25 percent is both the dielectric material and gaps.

14. SUBJECT TERMS artificial muscles, microfluidic capacitors, biomimetic	**15. NUMBER OF PAGES** 79
	16. PRICE CODE

17. SECURITY CLASSIFICATION OF REPORT	**18. SECURITY CLASSIFICATION OF THIS PAGE**	**19. SECURITY CLASSIFICATION OF ABSTRACT**	**20. LIMITATION OF ABSTRACT**
Unclassified	Unclassified	Unclassified	UU

NSN 7540-01-280-5500

Standard Form 298 (Rev. 2-89)
Prescribed by ANSI Std. 239-18

THIS PAGE INTENTIONALLY LEFT BLANK

Approved for public release. Distribution is unlimited.

MODELING AND SIMULATIONS FOR OPTIMIZATION OF MICROFLUIDIC MICROCAPACITOR ARRAYS OF BIOMIMETIC ARTIFICIAL MUSCLES FOR QUIET PROPULSION AND EXOSKELETAL LOCOMOTION

Joshua M. Keeven
Captain, United States Marine Corps
BS, Purdue University, 2016

Jacob M. Leckie
Captain, United States Marine Corps
BS, Montana State University, 2013

Submitted in partial fulfillment of the
requirements for the degree of

MASTER OF SCIENCE IN MODELING, VIRTUAL ENVIRONMENTS, AND SIMULATION

from the

NAVAL POSTGRADUATE SCHOOL
June 2022

Approved by: Emil P. Kartalov
Advisor

Amela Sadagic
Co-Advisor

Quinn Kennedy
Second Reader

Gurminder Singh
Chair, Department of Computer Science

THIS PAGE INTENTIONALLY LEFT BLANK

ABSTRACT

The technology that we focused on was the biomimetic actuation of microfluidic microcapacitors, which are electrostatically actuated structures that contract and function like biological muscles. Our thesis aims to find the optimal muscle-to-tendon ratio while expanding both the standard and gap design arrays and to find the respective force-density saturation values so predicted force output can be calculated for muscle fibers of a practical size. We also studied if a 3D virtual object can be a suitable model for the human operators' examination of the artificial muscle and the optimization of its structure. Our results showed a maximum force density saturation of 8800 Pa and 6700 Pa when simulating the standard and gap array respectively with planar polarity wired artificial muscles. The optimal muscle-to-tendon ratio from the data gathered on the standard array simulations is approximately 9 to 1, meaning 90 percent of the surface area of the XY plane represents microfluidic capacitors and 10 percent is dielectric tendon material. The optimal muscle to tendon ratio from the data gathered on the gap array simulations is approximately 75 to 25, meaning 75 percent of the surface area of the XY plane are microfluidic capacitors, and 25 percent is both the dielectric material and gaps.

THIS PAGE INTENTIONALLY LEFT BLANK

TABLE OF CONTENTS

LIST OF FIGURES

LIST OF TABLES

THIS PAGE INTENTIONALLY LEFT BLANK

EXECUTIVE SUMMARY

Artificial muscles have played a vital role in the development of soft robotics. The U.S. military has recognized the potential benefits in creating lightweight and power-efficient actuators, which are devices that convert energy into physical movement [1]. The artificial muscle technology that we focused on was the biomimetic actuation of microfluidic microcapacitors, which are electrostatically actuated structures that contract and function like biological muscles. The reason we decided to explore this technological area is the materials and scale required to make such a device would be practical with state-of-the-art additive manufacturing technology that has become available only recently. This technology has the potential to overcome many of the restricting factors present in other forms of actuation and find innovative applications in underwater stealth propulsion, exoskeletons, and prosthetics as outlined in [1].

This thesis builds upon the research highlighted in [1], which used COMSOL software to simulate 3D printable models of microfluidic capacitors that generate electrostatic forces between capacitor plates and then transfer the force to the world via tendons comprised of the dielectric material between columns of capacitors. Our thesis aims to find the optimal muscle-to-tendon ratio while expanding both the standard and gap design arrays and finding the respective force density saturation values so predicted force output can be calculated for muscle fibers of a practical size. We also studied if a 3D virtual object can be a suitable model for the human operators' examination of the artificial muscle and the optimization of its structure. We used COMSOL, a physics simulation software and the Hamming Cluster Computing resources, to create and simulate 3D models to calculate the optimal dimensions of the artificial muscle design and used the insight gained from the visualized force and deformation post-simulation models to make design changes. After completing the standard array simulations, we found that the muscles were deforming in a way that might benefit from adding air gaps between the muscle fibers; this allows the dielectric material to bulge into the air gaps during compression caused by the electrostatic forces experienced between the muscles' capacitor plates. Our results showed a maximum force density saturation of 8800 Pa and 6700 Pa when simulating the standard and gap

array, respectively, with planar polarity wired artificial muscles. The optimal muscle-to-tendon ratio from the data gathered on the standard array simulations is approximately 9 to 1, meaning 90 percent of the surface area of the XY plane represents microfluidic capacitors and 10 percent is dielectric tendon material. The optimal muscle-to-tendon ratio from the data gathered on the gap array simulations is approximately 75 to 25, meaning 75 percent of the surface area of the XY plane contains microfluidic capacitors and 25 percent comprises both the dielectric material and gaps. We also determined that COMSOL-generated 3D virtual objects were a suitable model for the human operator to examine the artificial muscle models and make decisions about further optimization of their structure. For future work, we recommend that the air gap size, wiring configuration, and external geometry be manipulated and optimized to improve the standard array's benchmark saturation values.

References

[1] M. A. Coltelli, J. Catterlin, A. Scherer, and E. P. Kartalov, "Simulations of 3D-Printable biomimetic artificial muscles based on microfluidic microcapacitors for exoskeletal actuation and stealthy underwater propulsion," *Sensors and actuators. A. Physical.*, vol. 325, p. 112700–, 2021, [Online]. Available: https://doi.org/10.1016/j.sna.2021.112700.

ACKNOWLEDGMENTS

We would like to acknowledge Dr. Emil Kartalov for the idea and applicability of his design while we expanded on and implemented the work conducted in this specific area of modeling the physics of the outlined artificial muscle system. We would also like to acknowledge Michelangelo Coltelli, who was instrumental in setting up the initial COMSOL models so that they functioned in a logical way in accordance with the physics of the simulation software. His assistance was also critical for debugging and fixing issues with new designs as they emerged and provided help in navigating the COMSOL system even after he moved away from NPS. We would be remiss if we did not acknowledge Dr. Paul Leary and Dr. Jeffrey Haferman for their patience, direction, and guidance in personally working with our code and COMSOL models to allow us to leverage the computing power of the Hamming Cluster Computer to calculate and evaluate our artificial muscle physics simulations.

THIS PAGE INTENTIONALLY LEFT BLANK

I. INTRODUCTION

A. RESEARCH DOMAIN

The research domain of this thesis is the simulation of force density outputs for 3D-printed artificial muscles. We are focusing on the technology that merges additive manufacturing and electrostatically actuated devices and enables replication of human muscle and tendon systems. Our work uses 3D modelling and the COMSOL simulation software to design and simulate various structures and generate numerical and visual results that allow the optimization of the artificial muscle structure.

B. RESEARCH PROBLEM AND MOTIVATION

Commonly used forms of actuation suffer from disadvantages that make them impossible or impractical for very small-scale devices such as requirements for large surface areas or excessive energy inefficiencies. Electrostatic actuation offers energy-efficient and scalable solutions for very small devices that could be 3D printed as artificial muscles. The United States military has recognized the potential benefits of creating lightweight and power-efficient actuators which are devices that convert energy into physical movement [1]. The artificial muscle technology that we focused on was the biomimetic actuation of microfluidic microcapacitors which are electrostatically actuated structures that contract and function like biological muscles. The reason we decided to explore this technological area is because the materials and scale required to make such a device would only be practical with state-of-the-art additive manufacturing technology that has become available only recently. This technology as shown in [2] has the potential to overcome many of the restricting factors present in other forms of actuation and find innovative applications in underwater stealth propulsion, exoskeletons, and prosthetics. Coltelli et al. have experimented with conceptual models in [2] to create a biomimetic electrostatic form of robotic actuation that has the potential to be significantly more efficient than traditional means. Due to their achievable complex fluid motions, biomimetic artificial muscles have the potential for application in medical prosthetics, military exoskeletons, and acoustically quiet underwater propulsion systems as stated in [2]. Coltelli

et al. used COMSOL software to simulate models of microfluidic capacitors connected in parallel and optimize the model's dimensions to produce a design with the greatest force density because when a voltage is applied to a capacitor, its plates experience an attractive force that scales as the inverse square of the distance between the plates as outlined by Coltelli et al. [2]. Similar to human biology, the simulated muscles generate the force via the electrostatic force between capacitor plates and then transfer the force to the world via tendons that are the dielectric material between columns of capacitors.

The study's results primarily dealt with optimizing a 2x2x1 capacitor array. The study presented in [2] found that the maximal force density of a 1x1 array was 1.44 kPa while the maximal force density of a 2x2 array was 1.79 kPa. This suggests that the maximal force density of arrays will increase as they are expanded and eventually converge on a number used to determine the force output of macroscopic 3D-printed muscle fibers [2]. Constructing this saturation curve and determining the saturation value is one of the two goals of this thesis. Moreover, the saturation phenomenon itself, if confirmed, is of great practical utility as it would allow modest-size simulations to predict the behavior of far larger arrays of unit devices built at the same unit scale.

During simulation, it was observed that as the model contracted longitudinally, it also expanded laterally. With the concern that the model's longitudinal contraction was limited by its ability to expand, Coltelli et al. developed a model that left an air gap in between muscle fibers that would reduce the constraint on expansion [2]. The gap design has the potential to increase the force density output of artificial muscle fibers. The gap has not yet been simulated in the past and this thesis provides a study of its design. The size of the simulated arrays was limited due to computing power, and the prototypes were limited by outsourced 3D printing post-processing procedures. The lab has since acquired a much more powerful computer that allows simulation of larger arrays, and a 3D printer, namely the Stratasys Objet500, stated in [3] to allow for high-resolution printing of dimensions down to 100 microns. The Naval Postgraduate School's Hamming High Performance Computer (HPC) was available during this study. Exploring the effects of the gap design and optimizing its performance is the second goal of the current thesis. Simulation of the

gap design and derivation of the saturation force density can be accomplished with the same method used for the standard array design.

C. RESEARCH QUESTIONS

1. Will the force density of planar polarity wired artificial muscle arrays converge on a single value as the array is expanded longitudinally and laterally?
2. Will the optimal muscle-to-tendon ratio of planar polarity wired artificial muscle arrays converge on a single value as the array is expanded longitudinally and laterally?
3. Will the force density of planar polarity wired artificial muscle arrays with gap method converge on a single value as the array is expanded longitudinally and laterally?
4. Will the optimal muscle-to-tendon ratio of planar polarity wired artificial muscle arrays with gap method converge on a single value as the array is expanded longitudinally and laterally?
5. Is the three-dimensional virtual object a suitable model for the human operator's examination of the artificial muscle and optimization of its structure? Does the model convey enough information for the human user to understand how to optimize the models' parameters for a desired use?

D. SCOPE

This thesis focuses on finding the optimal muscle-to-tendon ratio and expanding both the standard and gap design arrays within the computational limits of the lab's and HPC's computers. The goal is to determine if and at what size the maximal force density output converges, so that predicted force output can be calculated for muscle fibers of a practical size. This thesis is conducted primarily with COMSOL software, and the corresponding physical prototypes are not made. The optimal muscle-to-tendon ratio is determined by conducting a parametric sweep of parameter u, which is the width of dielectric material between columns of capacitor plates and L, the width of the air gap. The

optimal u and L width is determined for their respective models by which u and L dimensions yield the highest force density after force density convergence. Force density convergence is determined once the increase in max force density becomes negligible with respect to the max force density of the previous array size.

E. METHODOLOGY

The models created without a gap are referred to as the standard model while the models that include air gaps are referred to as gap models. The planar polarity of wiring refers to making all capacitor plates on the same y plane (horizontal reference plane within COMSOL 3D modeling software) have the same positive or negative charge. The methodology entailed the following steps:

1. Conduct literature review of the past work in domain of our study, including electrostatic actuation, Objet500 Connex3 3D printer, COMSOL capabilities, and physical properties of microfluidic capacitors.
2. Create COMSOL models of standard and gap arrays with dimensions according to the 3D printer's manufacturer guidance.
3. Expand the models to create models for both the standard and gap arrays.
4. Design a set of experiments that will address all research questions.
5. Design the models to support Experiment 1 and 2: (1) Create larger models and simulate by expanding the array laterally and longitudinally until force density output converges or computational limits are reached. (2) Create virtual 3D model and examine its suitability for human operator data exploration and optimization of 3D model structure.
6. Conduct Experiment 1: Simulations of standard arrays will provide data needed to answer research questions 1,2 and 5.
7. Conduct Experiment 2: Simulations of gap method arrays will provide data needed to answer research questions 3,4 and 5.

8. Analyze data sets collected in both experiments: Analyze the force density data for each array size and develop a suitable visualization of the resulting data set for each model.

9. Make recommendations for future work.

F. THESIS STRUCTURE

1. Introduction: Description of Microfluidic Microcapacitor Arrays for Biomimetic Artificial Muscles for Quiet Propulsion and Exoskeletal Locomotion, to include the problem statement, motivation, scope, and thesis outline

2. Background: Literature review.

3. Methodology: List of the steps applied to the problem space that allowed us to address all research questions. We highlight potential challenges the project and idea might face.

4. Experimentation: Detailed description of the experiments, apparatus, procedures, and approaches used to build the simulation and collect data.

5. Results: The raw data and results of our simulations, tests and visualizations.

6. Discussion: The analysis of the results, the statistics and the interpretation of the results.

7. Conclusions.

8. Way forward: Future works, questions and direction.

THIS PAGE INTENTIONALLY LEFT BLANK

II. BACKGROUND

A. ARTIFICIAL MUSCLE BACKGROUND

Artificial muscles are not a very recent topic, as the work in that domain was initiated over seventy years ago. The first artificial muscle built was in 1950 and is attributed to atomic physicist Joseph Laws McKibben in [4]. In some of our earlier reading into artificial muscle, the conference paper "Review of Artificial Muscle Approaches" [5] outlined the performance and versatility that natural muscle possesses and how we are able to produce a muscle that can surpass natural muscle at specific benchmarks in performance, but there is still no artificial muscle that can exceed a natural muscle in all its aspects. The review [5] goes on to outline the basic natural muscle structure and artificial muscle performance parameters. There is a limit to how many comparisons we can make from natural muscle to artificial when we start looking deeper into the actual structure of the muscle itself; for example, natural muscle can repair itself stronger when actuated under loading, the exact opposite is true of the artificial variety.

B. ARTIFICIAL MUSCLE TYPES AND PRODUCTION

Artificial muscles can be organized in several large groups: electroactive polymers, thermal actuators, pneumatic artificial muscles and piezoelectric, broadly categorized by [2]. We will briefly outline the main characteristics of each group.

1. Electroactive Polymers

Electroactive polymers have similarities to biological muscles in that they are actuated when an electric field is applied. However, this method of actuation with current material technology has very low efficiency and durability. Manufacturing complexity is also very high leading to obvious problems of scalability, production, and cost for any practical application. A method of production has been put forward for very specific applications where a single die can be used to produce multiple actuators [5]; however, direct correlation to the method of load transmittal is limited. As a visualization aid, Figure

1 shows an example of an electroactive polymer experiment conducted by J. Paquette and K. Kim in their IEEE journal article [6, Fig. 1].

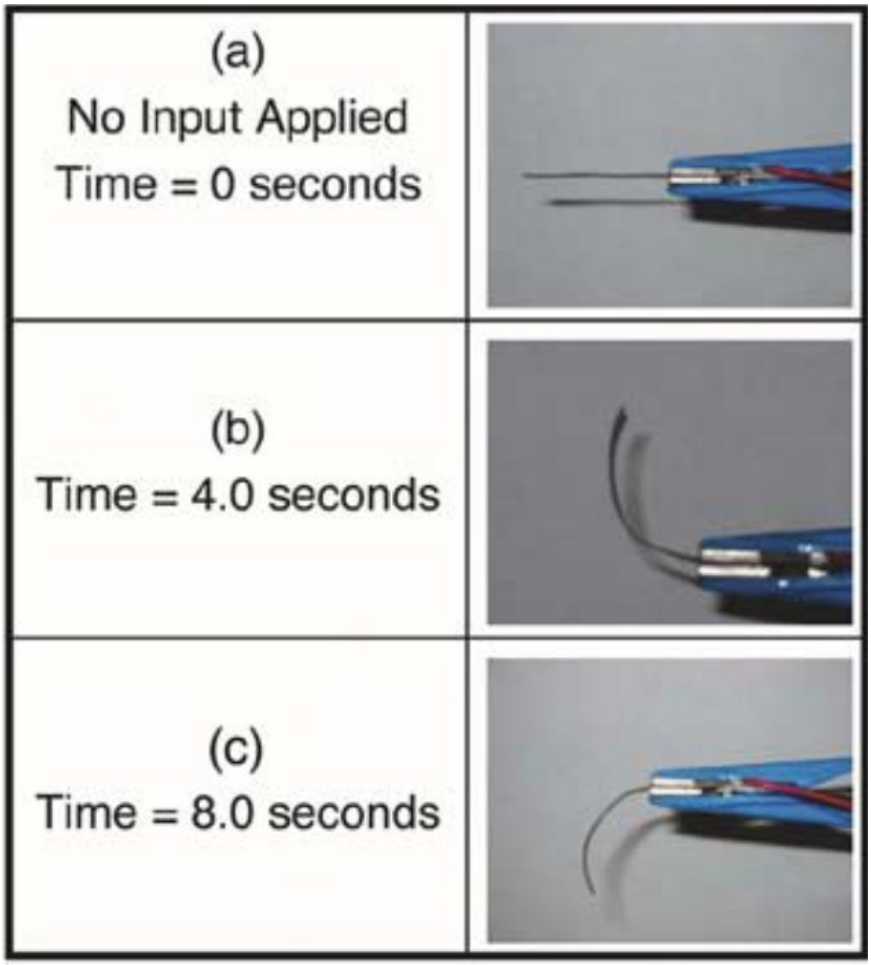

Figure 1. Standard ionic polymer–metal composite under 4 second step function voltage for full deflection. Source: [6].

2. Thermal Actuators

Thermal actuators include anisotropic metals that bend when heated and shape memory alloys [7]; both have a better range of actuation and can exert greater force outputs than electroactive polymers. However, thermal actuators do suffer from semi-complex production methods that drive up costs. The primary downside is that thermal actuators need to be heated to varying and specific temperatures to actuate, which severely impedes

the cycle time and reaction of actuation. This, unfortunately, makes them impractical for most forms of biomimetic locomotion. For clarity, Figure 2 highlights a textbook example of a thermal actuator in an experiment conducted by P-J. Cottinet et al. [8, Fig. 11] showing the change in displacement of a thermal actuator when voltage is applied.

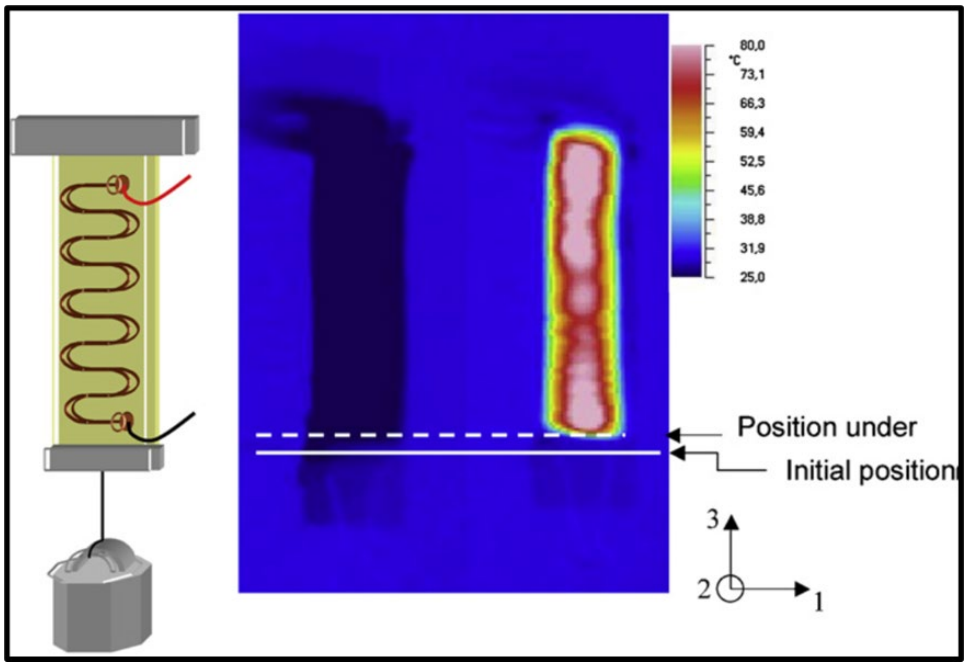

Figure 2. Example of unheated thermal actuator (left) and infrared imagery (right) showing the contraction of the polymer under induced heating as conducted. Source: [8].

3. Pneumatic Actuators

Pneumatically actuated artificial muscles fall into many specific types; the simplest example, as described in [9], and is basically a sack that can be filled with an incompressible liquid and encased in flexible fibers in various configurations for different loading conditions. When the sack is filled, it creates tension in the fibers and simulates a real muscle. This system is limited similarly to pneumatics and hydraulics in that they are hard to scale and are limited in the level of control attainable, as detailed by Liptak in Chapter 3 of the *Instrument Engineers' Handbook* [10]. He further outlines the differences in digital, electrical, hydraulic, and solenoid actuators in Chapter 6 of the same book. As a

demonstration, Figure 3 shows an example of the flexing of an extensor bending pneumatic artificial muscles designed and tested by H. Al-Fahaam et al. in their paper [11, Fig. 3] studying the application for hand augmentation and rehabilitation.

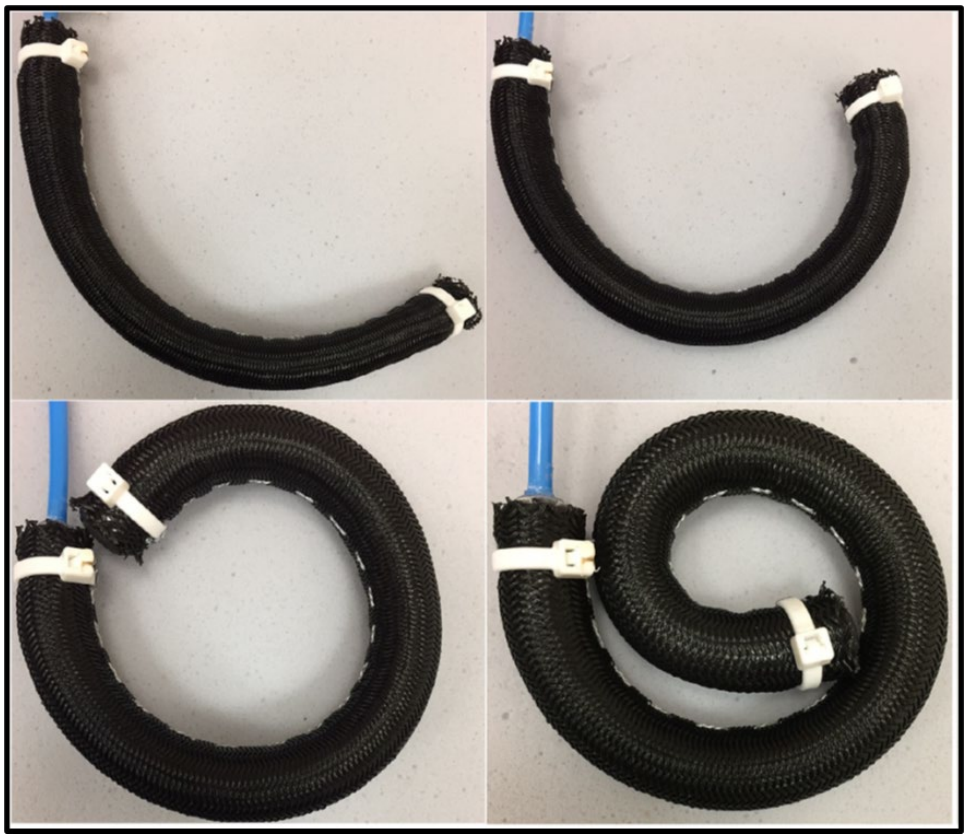

Figure 3. A pneumatic artificial muscle. Pressure at level 1 (upper left), pressure at level 2 (upper right), pressure at level 3 (lower left), and at level 4 (lower right pressure). Study did not release actual pressure data. Source: [11].

4. Piezoelectric Actuators

Piezoelectrics are by far the least used in the realm of artificial muscles or mechanical locomotion and actuation; the reason for that is predominantly their very small range of motion. The domain in which the piezoelectrics excel are the situations when they offer a relatively large amount of force for the low applied voltage, relatively speaking, and for a much shorter actuation cycle. Piezoelectrics are still one of the very few artificial

muscles that can be produced and utilized in the field of micro and nanotechnology for actuation [12]. Piezoelectrics like electroactive polymers also suffer from complex and difficult manufacturing processes leading to substantial scalability issues and impractically high costs, as specified in [13]. To clearly outline the differences between conventional and shape memory piezoelectrics and also depict the execution of a piezoelectric actuator we see in Figure 4, where T. Higuchi et al. [14, Fig. 13.2] clearly outlines the comparison.

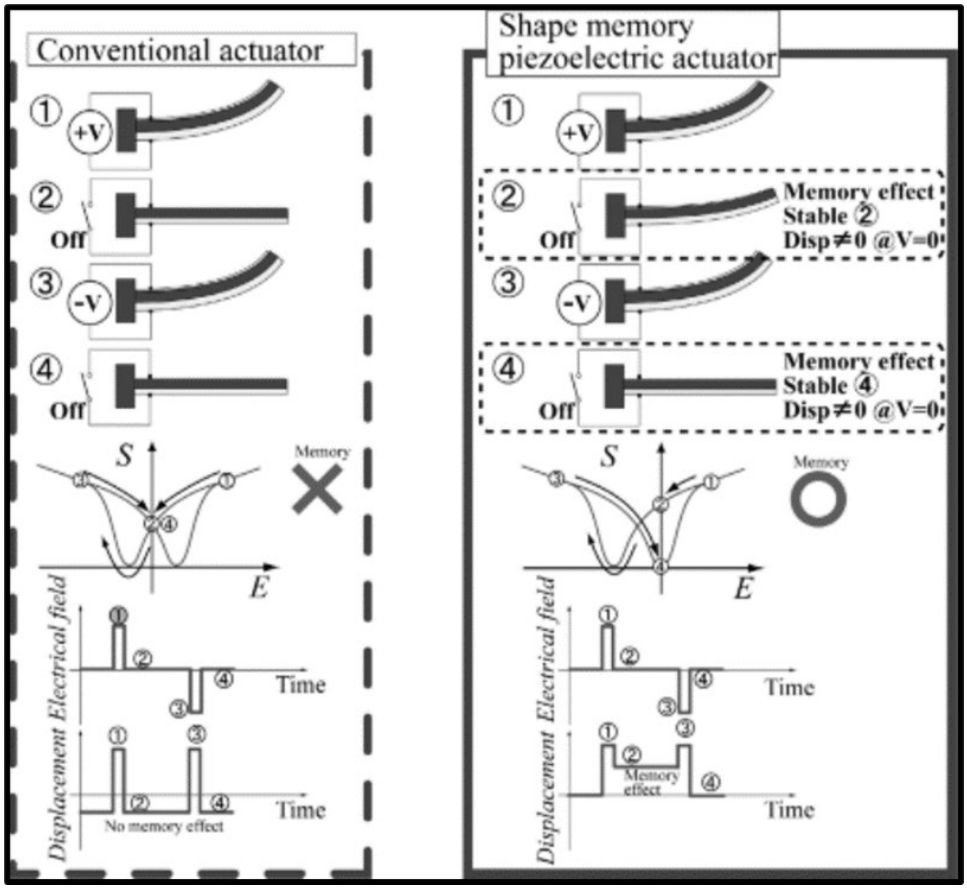

Figure 4. Conventional piezoelectric actuator (left)with its associated displacement and electric field. The difference (right)when using shape memory piezoelectrics and how the displacement changes compared to the conventional. Source: [14].

5. Dielectric Elastomer Actuators

Dielectric Elastomer Actuators can technically be grouped in with electroactive polymers, since the elastomer between the charged plates is deformed and rebounds as a partial actuation source, [15] highlights that. The force driving primary actuation is macroscopically situated to capitalize on the scale of the electrostatic force that scales as the inverse square of the distance between the charged plates. The problem remains in manufacturing small enough arrays of dielectric elastomers and charged plates as traditional methods involve similar methods to piezoelectric and electroactive polymers.

6. Liquid-Crystal Elastomer

Liquid-crystal elastomer (LCE) soft robots and devices are muscles layered with an electrothermal film which under low driving voltage demonstrate an electrothermal effect and have shown to be capable of relatively high force density and promise in recent years as a method of electrically actuated soft artificial muscle, as seen in [16]. We determined that LCE's and their application were close in size and scope to the type of actuation, direction, forces and application of interest. Fabrication of LCEs that are layered with an electrothermal film is a series of semi-complex steps involving the application of a polydimethylsiloxane (PDMS) template pressed onto a polyimide film. The film must be irradiated for a specific time at a precise wavelength of ultraviolet light. After this, a scalpel is used to wade and drag a composite solution multiple times into the micro trenches created by peeling the film away from the PDMS template. The film is finalized on a hot plate for a certain time and temperature to evaporate the solvent. Similar to LCE's we see a newer concept that is similarly constructed and similarly difficult to build being the electrostatic zipping actuators which like LCE's require the layering of a ferrite material between two non-conducting sheets as described in [17]. Electrothermal performance controlled by an external voltage for the LCEs layered with an electrothermal film was tested at 6.5 volts for a saturation temperature of 189 °C that was reached with a heating rate of 21 °C/s as demonstrated in [16]. These results allow the soft artificial muscle to execute a semi-quick and significant contraction. For the actuation and controllability of the soft artificial muscle there is an applied voltage to the LCEs, and they saw better results

with an increase from 3.5 volts to 6.5 volts at intervals of 1 volt. Utilizing an identical heating time of 20 seconds, the maximum actuating stress in the liquid crystal elastomer film increased almost linearly. They found that when the time was extended to 30 seconds, they achieved an actuating stress on the LCEs film of 0.46 MPa. This is about 31% higher than that of mammalian skeletal muscles which achieve actuating stress at roughly 0.35 MPa as tested in [16]. There were some identified items that would require more research, the first of which being the slow responsiveness of the LCEs when the voltage was turned off. This slow responsiveness occurred after the initial voltage had caused the flexion. The LCE's recovery time of around 87 seconds was almost "7 times longer than the actuating time" as part of the study done in [16]. This lag in the recovery process is thought to be mainly attributed to the slow cooling speed of liquid crystal elastomers via air conduction, which is similar to the above explanation concerning "different thermal transfer types of soft artificial muscles during the actuation and recovery processes" [16]. One of the disadvantages inherent to the process required to fabricate LCEs layered with an electrothermal film, and their use in actual application, is that the system is highly temperature-dependent which [16] highlighted. For example, the muscles would need to be manufactured for a specific temperature range or area of operation, provided one was following the example of robotic fish and how water temperature impacts both the cycle rate and range of motion in their artificial muscle. Likewise, similar electrostatic zipping actuators would need to be purpose assembled for the specific application and temperature range as the thin non-linear shape of the layers will be severely impacted by temperature as we see in [17]. A secondary disadvantage of this technology and its application is the manufacturing scalability. Many layered LCEs of the same size could theoretically be built up together to form a stronger muscle. Unfortunately, the external electrothermal films would cool much quicker than the ones on the inside. With the level of flexion being severely temperature-dependent for a full range of motion, a great deal of shear stress would accumulate at the boundaries of where one LCE was layered against another. The same is again true of the electrostatic zipping actuators, and well stated by Szkopek et al. "the distance for which the pull-in effect occurs is variable, depending on the length, thickness, weld width and initial deflection of the actuator. This phenomenon turns out to

be so important that in extreme cases it may limit the range of stable muscle control from ~ 35% to ~ 11% of its total strain." The final, albeit partial, disadvantage to the system is that for the artificial muscle to remain at full flexion, the system requires continual voltage to maintain the required level of heat. On the plus side, no power is required to bring the muscle back to its unflexed state, but management and dissipation of heat from the system would be a significant hurdle in practical implementation. Our research is to find a similar solution that solves the issue of stationary power requirements and ease of manufacturing.

C. ARTIFICIAL MUSCLE TYPE APPLICATIONS

The two most popular subsets of the overarching topic of artificial muscles in general are robotic artificial muscles as delineated in [18] and exoskeletal locomotion artificial muscles, both typically accomplished via pneumatics, hydraulics and or electric servomotors. Pneumatics and hydraulics are the primary locomotion devices in large application areas such as assembly lines and construction vehicles since in larger sizes they have tremendous strength and produce little to no heat at the site of actuation. There are some drawbacks to pneumatics and hydraulics in that they require a compressor and do not scale well for smaller systems as we see in [19]. The fundamental reason they are not used in smaller exoskeletal applications is the difficulty in producing smooth, intricate, organic motion due to the semi-binary nature of the fluid switches [2]. Electric servomotors have better miniaturization potential than pneumatics and hydraulics, which makes them the better choice for smaller scale applications. Some of the drawbacks for electric servomotors are that they require the generation of a strong magnetic field which if accomplished via solenoids can require high current requirements, which in turn produces a great deal of heat at the site of actuation, while the generated heat decreases overall power efficiency. Biomimetic artificial muscles based on microfluidic microcapacitors and electrostatic actuation are the subject of active research through a variety of approaches. "Practical artificial muscles are highly desirable in a wide range of applications, including strength augmentation in military exoskeletons, medical prosthetics for amputees, locomotion boosters for geriatric and handicapped patients, walker robots, and acoustically quiet underwater propulsion systems" [2].

D. 3D PRINTING

Throughout our research in this domain, we continued to identify the same types of problems in most of the current designs in artificial muscles regarding scalability and cost-effective production of artificial muscle. Many designs seemed to remain in the realm of basic science and not translated over to real world application. That is most evident in examples like the electrostatic zipping actuators [17] and the ratchet-integrated pneumatic actuator [19]. In our experience, for an artificial muscle to be more than an interesting lab experiment and instead become applicable to the real world and even have military applications, there needs to be both a focus on production in the design phase and a focus on leaderships guidance on systems, that are invested. One way of manufacturing the structures with complex geometry, in a variety of materials, and doing it in a cost-effective way, even on a small scale (small number of items), is by using 3D printing or additive manufacturing (AM). The Marine Corps order concerning AM policy the Commandant of the Marine Corps states that, "The Marine Corps is embracing emerging technologies by incorporating additive manufacturing (AM) methods to prototype and produce repair parts and innovative solutions" [20]. The focus of this thesis and research is not on advancing AM technology or the myriad of advantages and disadvantages associated with it. Instead, the focus of the research is on AM applications for artificial muscles while addressing the scalability, manufacturability, and modularity needs of artificial muscles in the areas of exoskeletal actuation and stealthy underwater propulsion.

E. ARTIFICIAL MUSCLE AND 3D PRINTING

We discussed some of the perceived and real drawbacks identified in the artificial muscles in industry today and some solutions. One method involves the clever combination of the above-mentioned electrostatic actuation of microfluidic capacitors combined with the flexibility of additive manufacturing. The proposed resulting stress generated is estimated at 33 MPA with current manufacturing techniques. To further the theoretical study of the proposed system a program named COMSOL was utilized to simulate the 2x2x1 array of the proposed device. The results showed the feasibility of the proposed idea as COMSOL accurately outputs the desired behavior. Several performance maximizing

design values were derived from executing parameter sweeps of the 2x2x1 array to generate more ideal force density [2]. The added ability of the microfluidic microcapacitors to stay flexed while not expending any power is almost unrivaled in the artificial muscle industry with only one other alternate, a pneumatic actuator with a combined mechanical device for maintaining flexion [19]. The potential applications of rapid and easy scaling in manufacturing, good force outputs and biomimetic architectural flexibility will have massive impacts in the areas of acoustic translucent underwater propulsion and exoskeletal locomotion. This thesis will focus on expanding the developments of microfluidic microcapacitors designed to be produced via 3D printing for the application of biomimetic actuation and propulsion.

F. CHAPTER SUMMARY

This chapter documents the literature that we reviewed and the important information we learned prior to starting our study. We highlight literature that outlined some of the fundamentals of research in the domain of various types of artificial muscles on the market, how the various artificial muscles are produced, the importance of considering manufacturing and cost in the design phase, biomimetic actuation and microfluidic microcapacitors.

III. METHOD

A. PHYSICS AND MATHEMATICS

The primary source of force generation in our study is electrostatic actuation. The two sources of attractant forces are two square capacitor plates, one charged positive and the other negative. The study focuses on the miniaturization of the capacitors and building them in a 3D array to study the forces exerted on the model. For the sake of simplifying the simulation model, we will be treating the two plates as a near perfect capacitor with some of the complicated edge effects not represented to secure flexibility and simplicity in the simulation math.

One of the first equations in most electrostatic primer textbooks concerns the electrostatic fields generated by one of the plates in a vacuum. The electrostatic field E is described in [2] as

$$E = \frac{\sigma}{2*\varepsilon_0} = \frac{Q}{2*\varepsilon_0*A}, \quad (1)$$

where the surface charge density is σ, the charge in the single plate is (Q), and the area of the single plate is (A). The total force (F) induced on the other plate by the electric field via the induced charge in the other plate is described in [2] as

$$F = Q * E = Q * \frac{Q}{2*\varepsilon_0*A} = \frac{Q^2}{2*\varepsilon_0*A}. \quad (2)$$

We are modeling the dielectric as perfectly linear between the plates for mathematical simulation simplicity. The dielectric constant we will introduce is ε_r. so that F is described in [2] as

$$F = \frac{Q^2}{2*\varepsilon_0*\varepsilon_r*A}. \quad (3)$$

From another direction, we consider the capacitance of the parallel plate capacitors under the assumption of perfectly linear dielectric between the plates for mathematical simulation

simplicity. Where the applied voltage is (V) and the distance between the parallel capacitor plates is (D). Capacitance, C, is described in [2] as

$$C = \frac{Q}{V} = \frac{\varepsilon_0 * \varepsilon_r * A}{D}, \tag{4}$$

where the edge effects are neglected for a parallel-plate capacitor. Use of this formula is justified, because the microcapacitors we are modelling have dimensions where the length and width of the plates is large compared to the thickness of the dielectric between the plates.

The total force with capacitance inserted, F, is described in [2] as

$$F = \frac{\left(\frac{\varepsilon_0 * \varepsilon_r * A}{D}\right)^2}{2 * \varepsilon_0 * \varepsilon_r * A} \xrightarrow{algebra} \frac{\varepsilon_0 * \varepsilon_r * A * V^2}{2 * D^2}. \tag{5}$$

As this is a series of devices set up in an array, the parameter that we are really interested in is the force density (f) or how much force per unit area the device can generate as described in [2] as

$$f = \frac{F}{A} = \frac{\left(\frac{\varepsilon_0 * \varepsilon_r * A * V^2}{2 * D^2}\right)}{A} \xrightarrow{algebra} \frac{\varepsilon_0 * \varepsilon_r * V^2}{2 * D^2}. \tag{6}$$

Coltelli et al. [2]. observed that to maximize the force density, one needs to minimize the distance between the plates. When we evaluated most manufacturing capabilities, in the interest of scalability of the system, it appeared that additive manufacturing is the ideal way to fabricate artificial muscles. Dr Kartalov's lab has a Stratasys Object500 Connex3 3D printer that will be used for future prototyping. Stratasys claims that the Object500 Connex3 3D printer has a 95% confidence tolerance of less than plus or minus 100 microns for the inside width of channels smaller than 100mm [21]. The 3d printer has a published vertical resolution of 16 microns and the manufacturer recommended no smaller than 100 micron dimensions for consistent results when printing in high quality mode.

The next factor to be considered in the realm of 3D printing is the voltage breech coefficient associated with the materials that can withstand our simulated voltages. For the

sake of simplifying the simulations, the model will be based on a semi-generic silicon with a breach voltage coefficient of around 885 V/μm. The initial constant values used for the start of the calculations were an initial voltage of 5 kV, the distance between the plates of 10 μm, and a dielectric constant of 3. With these values, the theoretical maximum force (f_{max}) can be determined for use as an upper bound in [2].

$$f_{max} = \frac{\left(8.85\times10^{-12}\frac{F}{m}\right)*3*(5000\ V)^2}{2*(10\times10^{6}\ m)^2} \cong 3.3\times10^{7}\ \frac{N}{m^2} \cong 33\ MPa \cong 4{,}815\ psi \qquad (7)$$

Substantial reductions in force density from the theoretical maximum force still project the pounds per square inch at 100 plus, which is sufficient even for the most demanding areas of artificial muscle use. During our research and the studies of Dr. Kartalov and his team, this combination of micro-fluidic capacitors and additive manufacturing techniques has yet to be attempted, even though other researchers have worked on electrostatic actuation. The fundamental reasons for l between fibers averaging the strengths of 3D printing are the speed and precision of manufacturing and the ability to create structures otherwise impossible by other means. The microfluidic capacitors will be 3D printed with channels filled with conductive gel or liquid to make up the control wiring for the system. The bulk dielectric that the printer would print would make up the mechanical medium of force transfer, and this is one of the material limitations in prototyping as the generic printable dielectrics are not optimized for these types of systems but will serve as a baseline for initial tests. We see this as a truly unique and efficient method of building artificial muscles that meet the requirements of the DOD in motion distance, force output, manufacturability, scalability, and biomimetic architectural flexibility.

B. CHAPTER SUMMARY

In this chapter we outlined the fundamental equations and rough calculations that make up the basis for how COMSOL is evaluating the force output of the simulated artificial muscle.

THIS PAGE INTENTIONALLY LEFT BLANK

IV. EXPERIMENTATION

A. INTRODUCTION

The following experiments have been designed to address our research questions listed in Chapter I, Section C.

Experiment 1: Conduct simulations of standard arrays to gather data on the force density output of various models to provide data needed to answer research questions 1,2, and 5.

Experiment 2: Conduct simulations of gap method arrays to gather data on the force density output of various models to provide data needed to answer research questions 3,4, and 5.

B. EXPERIMENT 1, STANDARD ARRAY

Experiment 1 is designed to answer our research questions 1, 2, and 5. We conducted parameter sweeps of the width of the tendon material in planar polarity wired artificial muscle models to determine the maximum force density output for each array until values converge in order to answer thesis question 1. We then determined what tendon width yields the highest maximum force density at convergence in order to answer thesis question 2. COMSOL software application is used to manipulate the 3D virtual object to create force distribution and deformation visuals and allow us to gather insight on how to optimize muscle structure in order to answer thesis question 5.

We began our research by recreating successful models from Coltelli et al. [2]. to ensure that our simulations had the same outputs and that we had a proper understanding of the COMSOL software. A table of parameters shown in Table 1 was created for the standard models to avoid manually building each array and instead make proportional relationships between the parameters so that increasing the array size would expand the overall structure to scale.

Table 1. Parameter definitions. This table shows the parameter values used to conduct the sweeps in COMSOL and corresponds to the parameters shown in Figure 5.

Parameter Name	Expression	Value	Description
e	u	1E-4 m	material on outside edges of structure
u	(100-200)[um]	1E-4 m	material in between fibers
D	plateY	1E-4 m	distance between plates
c	100[um]	1E-4 m	material on bottom and top of structure
plateX	1000[um]	0.001 m	capacitor plate x length
plateZ	1000[um]	0.001 m	capacitor plate z height
plateY	100[um]	1E-4 m	capacitor plate y length
Xarray	(1-14)	(1-14)	capacitor array x dimention
Zarray	10	10	capacitor array z dimention
Yarray	Xarray	(1-14)	capacitor array y dimention

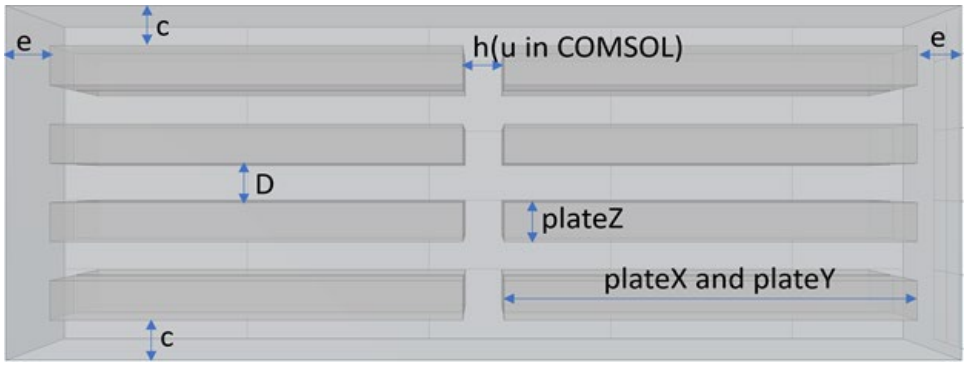

Figure 5. Schematic of model geometry with parameter definitions.

The tendon thicknesses at *e*, the device's left and right edges, and at *h,* between fibers were locked to be equal and swept together between 100 and 200 microns in steps of 10 microns. Top and bottom edge thickness c was set to 100 microns. The lateral widths (*plateX*, *plateY*) of microcapacitor plates were set equal to 1000 microns. Plate thickness (*plateZ*) and plate distance *D* were set equal to 100 microns. Array size NxNx10 was swept between N=1 and N=14 in steps of 1.

C. EXPERIMENT 2, GAP ARRAY

Experiment 2 is designed to answer our research questions 3, 4, and 5. We conducted parameter sweeps of the width of the air gap in planar polarity wired artificial muscle models with gap method to determine the maximum force density output for each

array until values converge in order to answer thesis question 3. We identified what gap width yields the highest maximum force density at convergence in order to answer thesis question 4. COMSOL application is used to manipulate the 3D virtual object to create force distribution and deformation visuals to gather insight on how to optimize the muscle structure for future work in order to answer thesis research question 5.

After evaluation of the standard array model by 3D inspection, as outlined in more detail later, we modified a functioning standard array model that we knew worked to include an air gap between each plate. A table of parameters shown in Table 2 was created for the gap models in the same way as the standard array model to avoid reconstructing each individual gap array and instead kept the proportional relationships between the parameters so that increasing the array size would expand the overall structure to scale.

Table 2. Parameter definitions. This table shows the parameter values used to conduct the sweeps in COMSOL and corresponds to the parameters shown in Figure 6.

Name	Expression	Value	Description
e	u	1E-4 m	Material on outside edges of structure
u	100[um]	1E-4 m	Material in between fiber and gap
plateX	1000[um]	0.001 m	plate x length
plateZ	1000[um]	0.001 m	plate z height
D	plateY	1E-4 m	distance between plates
c	100[um]	1E-4 m	Material on bottom and top of structure
plateY	100[um]	1E-4 m	plate y length
Xarray	2	2	array x
Yarray	10	10	array y
Zarray	Xarray	2	array z
L	100[um]	1E-4 m	Width of the gap

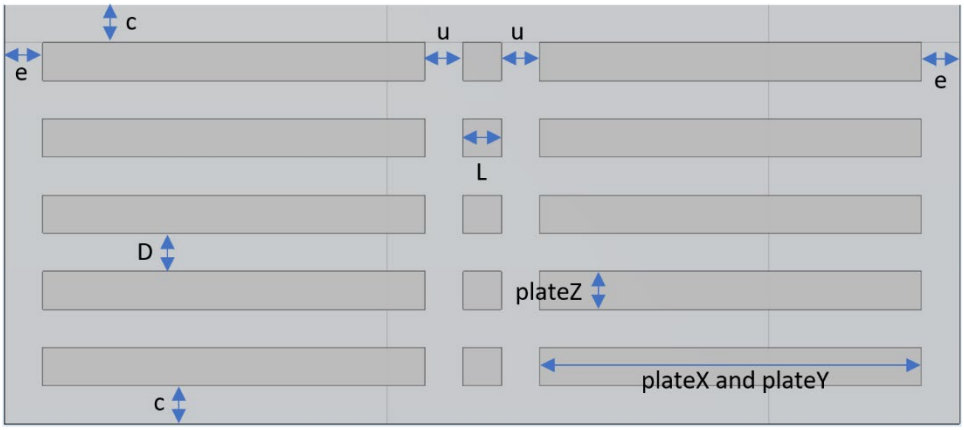

Figure 6. Schematic of gap model geometry with parameter definitions.

The tendon thicknesses, the device's left and right edges, e and the fibers between the gap L were locked to be equal and L was evaluated in increments in between 100 and 200 microns in steps of 10 microns. Top and bottom edge thickness c was set to 100 microns. Lateral widths (plateX, plateY) of microcapacitor plates were set equal to 1000 microns. Plate thickness (plateZ) and plate distance D were set equal to 100 microns. Array size NxNx10 was swept between N=1 and N=14 in steps of 1.

D. COMSOL MODELING PARAMETERS

Software: As conducted in [2], we also used COMSOL to generate the simulation models and parameter sweeps conducted in our study.

Structures: The basic structures of the model included the overall bulk material (Outer rectangular prism) and alternating pairs of electrode chambers (inner rectangular prisms) oriented in parallel within the dielectric, as depicted in Figure 5. These structures were joined together in COMSOL using the union function. Rectangular air gaps between the columns of capacitors are included in the gap models, as shown in Figure 6.

Material Inputs: Silicone PDMS was assigned to the bulk dielectric, specifically the material that would separate an electrode chamber from another electrode chamber, the material that would make up the tendon like areas between electrode chamber and the environment, the material that made up the space between the electrode chambers and the air gaps. Liquid water was assigned to all the electrode chambers, both the chambers

representing the grounded and positive plates are completely filled with liquid water. Air was assigned to the volumes modeled as compressible areas between tendons separated from each chamber by a distance equal to the tendon width in any direction.

E. MODEL MATERIAL PROPERTIES

The specific materials used and simulated in COMSOL are PDMS, water and air for simplicity of simulation. The material properties specifically used in our simulation are listed for repeatability in Tables 3, 4, and 5 respectively.

Table 3. Material properties of PDMS as shown in COMSOL used in the dielectric structure to model tendons, outer geometry, and the material between capacitor plates.

Relative permittivity	2.75	1
Density	970[kg/m^3]	kg/m³
Young's modulus	750[kPa]	Pa
Poisson's ratio	0.49	1
Coefficient of thermal expansion	9e-4[1/K]	1/K
Heat capacity at constant pressure	1460[J/(kg*K)]	J/(kg·K)
Thermal conductivity	0.16[W/(m*K)]	W/(m·K)

Table 4. Material properties of water as shown in COMSOL is used to model the conductive material in the capacitors.

Relative permittivity	80.1	1
Dynamic viscosity	eta(T[1/K])[Pa*s]	Pa·s
Ratio of specific heats	1	1
Electrical conductivity	5.5e-6[S/m]	S/m
Heat capacity at constant pressure	Cp(T[1/K])[J/(kg*K)]	J/(kg·K)
Density	rho(T[1/K])[kg/m^3]	kg/m³
Thermal conductivity	k(T[1/K])[W/(m*K)]	W/(m·K)
Speed of sound	cs(T[1/K])[m/s]	m/s

Table 5. Material properties of air as shown in COMSOL used to model the air gaps in the gap method models.

Coefficient of thermal expansion	alpha_p(pA,T)	1/K
Mean molar mass	0.02897[kg/mol]	kg/mol
Bulk viscosity	muB(T)	Pa·s
Dynamic viscosity	eta(T)	Pa·s
Ratio of specific heats	1.4	1
Electrical conductivity	0[S/m]	S/m
Heat capacity at constant pressure	Cp(T)	J/(kg·K)
Density	rho(pA,T)	kg/m³
Thermal conductivity	k(T)	W/(m·K)
Speed of sound	cs(T)	m/s
Parameter of nonlinearity	(def.gamma+1)/2	1
Specific gas constant	R_const/Mn	J/(kg·K)
Heat capacity at constant pressure	Cp(T)	J/(kg·K)
Ratio of specific heats	1.4	1
Mean molar mass	0.02897	kg/mol

Node Use: The three physics nodes that we used were the moving mesh, solid mechanics, and electrostatics. COMSOL is outfitted with two powerful solvers for the study of 3D geometry under various loading conditions. Deformed geometry and moving mesh can be used at the same time but they represent very different material controls. Deformed geometry foundationally involves calculations and simulations of removing or adding material to the original geometry. Moving mesh is used when a solid object under a specific load is deformed and how in our case fluid filled electrode and ground chambers react to the way the domain boundaries are displaced. The moving mesh node was applied to the bulk dielectric, the body of the electrode chambers, and the air gaps. As in the procedures used in [2], the solid mechanics node was applied to the bulk dielectric and by extension the surfaces of the electrode chambers and air gaps. The XZ plane at the zero Y position was also fixed in place as the primary displacement reference plane for the solid mechanics calculations. The fixed boundary node is parallel to the electrode plates, and all the other outsides of the bulk diametric were allowed to deform. We used the same methods as [2] and a “boundary load was applied to all surfaces of the model with the outputs for each component force being equated to their respective Maxwell Upward Surface Tension

Equations" that explain how electrical charges and currents produce magnetic and electric fields [2]. The boundary node is crucial for the model to work in conjunction with its interfaces because it connects the COMSOL physics nodes to impact the capacitive force interchange between geometry within the simulation. For the initial condition states, all boundary loads, and the mechanics of the linear elastic material were all defined and constrained in the solid mechanics node. The electrostatics node as outlined by COMSOL is where electric fields, potential distributions, and dielectrics can be evaluated at explicitly prescribed electric charge distributions. The electrostatics node was applied to all geometry and the initial values set to 0 Volts. Like in [2], within "the electrostatic node, a potential of 3000 Volts was applied to all surfaces of one of the electrodes, and a ground potential was applied to all surfaces of the other electrode." For the gap model, all air gaps between the dielectric material are assigned zero charge.

Derived Values: Following the procedure outlined in [2] "The output force of the device was calculated as the surface integral of the Von Mises Stress along the unconstrained outer surface of the device, opposite to the boundary-constrained surface. The total deformed surface area was calculated as the surface integral of the area of the unconstrained outer surface of the device, opposite the boundary constrained surface." The average output force density was calculated for each u parameter by dividing the total output force of the deformed surface by the total deformed surface area. From this data, the optimal muscle-to-tendon ratio can be determined for each model based on the u parameter that yields the highest force density.

The parameter N was utilized to define the dimension of the model during our study of both the standard and gap method arrays. The model was iterated from N=1 to N=14 at a step of 1 while the dimension of the model in the *z* direction remained constant. For context, the model had a dimension of NxNx10 relative to the X, Y and Z coordinate frame displayed in Fig. 7. For each N value, a parameter sweep of *u*, the material between columns of microcapacitors and material on outside edges of structure as displayed in Fig. 6, was conducted from 100 to 200 microns with a step size of 10 microns. After COMSOL completed the simulations, we compared the force density values from the sweep to determine what value of u would produce the greatest force density. After COMSOL

simulations were completed, the optimal value of u was determined for each model by plotting the force densities as a function of the swept tendon thicknesses. This process continued until saturation of max force density across all models was reached. Force density saturation was determined to be when the increase in max force density between models became insignificant as the maximal forces approached an asymptotic value as shown in Figure 8.

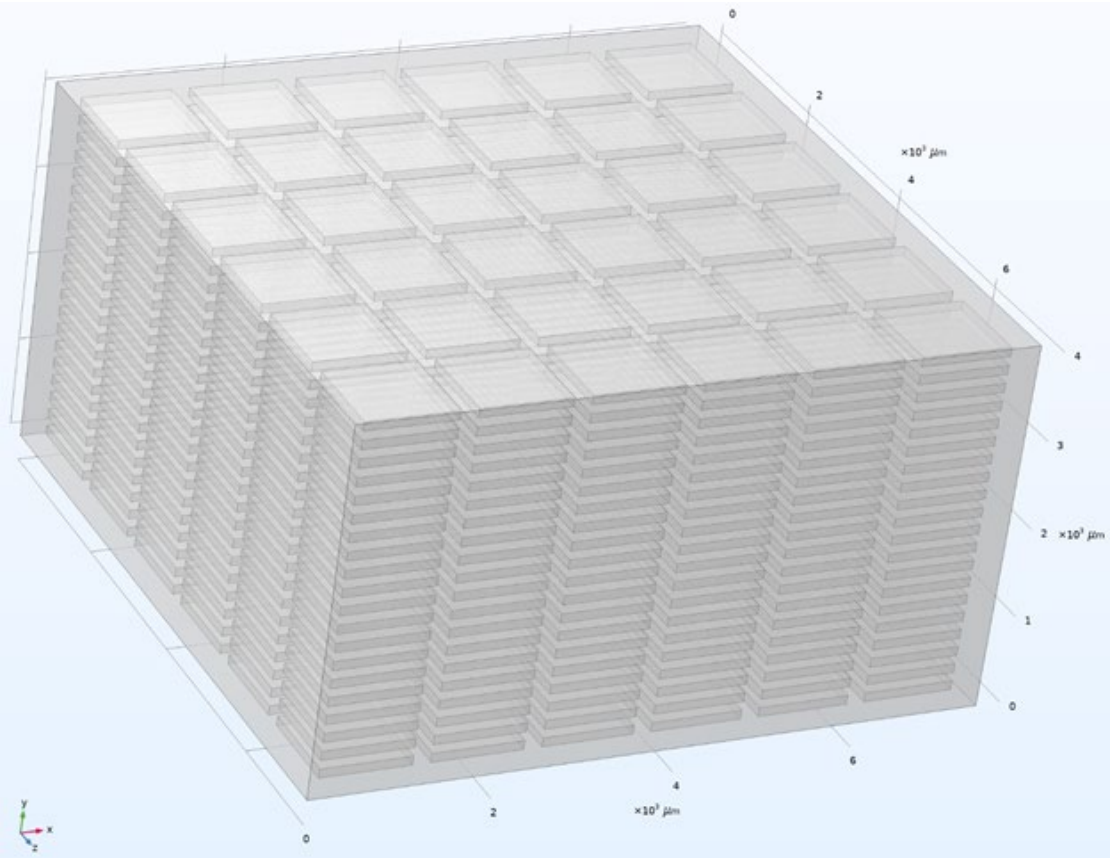

Figure 7. COMSOL Model of NxNx10 array where N=6

We started running simulations on the computer with small simulations of single parameter sweeps for an initial test and then conducted small simulations of multi parameter sweeps by expanding both the u parameter and the overall array size simultaneously. This was done by continuing to expand the models in the X and Y dimensions while keeping the Z parameter constant at 10 capacitor arrays.

F. HAMMING PROCESS AND METHOD

The computational requirements for the dense geometry in the COMSOL model required cluster computing. COMSOL can use distributed-memory parallel operations where each computing process is assigned parts of the total workload. This process also increases the total available memory which was the primary reason that our simulations of larger arrays failed on the lab computers. Small simulations could be run on a single node while learning on the Hamming Cluster, but larger jobs required batch submissions due to the long wait time associated with large resource requests. MobaXterm is a Secure Shell Protocol (SSH) terminal that we used to access the Hamming Cluster remotely and submit our batch files. Appendix A shows a sample of the file that we used to submit jobs and request resources. Resources from COMSOL's support page and NPS faculty members helped us to optimize the proper combination of nodes, Central Processing Units (CPU), memory, and time for each simulation job.

G. CHAPTER SUMMARY

In this chapter we outlined the COMSOL models, parameter definitions, and schematics of the model geometry for both the standard array and the gap array. We also outlined the COMSOL modeling parameters, both models' material properties and the process and method we went through to utilize the Hamming supercomputer.

THIS PAGE INTENTIONALLY LEFT BLANK

V. RESULTS

A. EXPERIMENT 1, STANDARD MODEL

The computational capacity of the lab computer with 16 cores was reached after simulating the 10x10x10 model. We found that the computation time increased linearly with the amount of geometry added to each model. For example, the 2x2x10 model had 40 pairs of capacitor plates, while the 3x3x10 model had 90 capacitor plates. When simulating the same number of u parameters for each model, the computation time of the 2x2x10 model was 4/9 the computational time of the 3x3x10 model. The longest simulation for the 10x10x10 model took approximately 4 days before we began using the NPS Hamming Cluster Computer for larger arrays. The code in Appendix A shows the nano file that we used to submit batch jobs to run our COMSOL simulations on Hamming. After experimenting with several different configurations, we found that the minimum resources to complete our COMSOL simulations for models up to 13x13x10 was 4 nodes with 64 cores each. The 13x13x10 simulation took 48 hours to complete on Hamming Cluster.

As can be seen from Figure 8, the max force density of expanding the N x N x 10 models laterally increases along an asymptotic curve that saturates around 8714.68 Pa which is produced when simulating the 12x12x10 model. When using our previous force density saturation criteria of less than a 2% change in max force density, we achieve saturation in the longitudinal direction at 12x12x12 with a value of 8808.56 Pa. The reason we chose 2% as our saturation criteria is because finding a more precise number would not be worth the time and computing resources. Stratasys claims that the Object500 Connex3 3D printer has a tolerance of 100 microns for the inside width of channels smaller than 100mm with a published confidence interval of 95% [21]. The printer has a published vertical resolution of 16 microns and the manufacturer recommended no smaller than 100-micron dimensions for consistent results when printing in high quality mode [21]. We stepped through the parameter sweeps of u in 100-micron increments which means the exact maximal force density for each model is likely in between parameter steps. Table 6 shows us that the 12x12x12 model with a u value of 110 microns should be a close

representation of the force density that can be expected with any larger model or 3D-printed device with a u value of 110 microns.

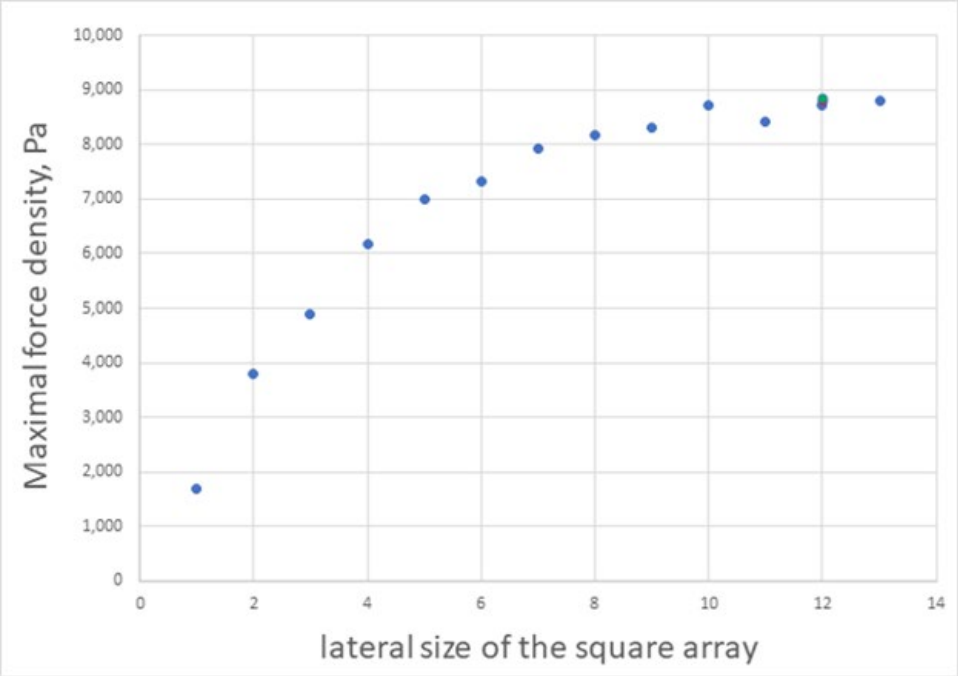

Figure 8. The max force density of N x N x 10 models where N equals 1 through 13. The red data point is a 12x12x11 model and the green data point is a 12x12x13 model.

Table 6. The max force density in pascals (Pa) and the corresponding u parameter that was used in the model.

Array Size	Max Force density, Pa	u param
1x1x10	1679.1678	100
2x2x10	3788.9375	110
3x3x10	4889.9450	140
4x4x10	6186.2934	120
5x5x10	6990.8797	130
6x6x10	7335.2858	130
7x7x10	7933.2855	110
8x8x10	8176.9907	120
9x9x10	8324.0317	120
10x10x10	8708.7806	120

Array Size	Max Force density, Pa	u param
11x11x10	8422.4528	100
12x12x10	8714.6854	110
13x13x10	8810.2280	100
12x12x12	8808.5573	110
12x12x13	8871.7639	110

From this data, we can answer thesis **research question 1**: The force density of planar polarity wired artificial muscle arrays converge on a single value around 8800 Pa or 1.28 PSI as the array is expanded longitudinally and laterally. From this data we can also answer thesis **research question 2**: The optimal muscle-to-tendon ratio from the data gathered on the standard array simulations is approximately 9 to 1, which means that 90 percent of the surface area of the XY plane are microfluidic capacitors, and 10 percent is dielectric material. Since the electrostatic force between the plates scales as the inverse square of the distance between the plates, we believe that much larger forces can be achieved by scaling the model down to smaller sizes once additive manufacturing technology advances. As we can see from Figures 9, 10, 11, and 12, simulated structures bulge out laterally and appear to limit the amount that the structure can compress longitudinally. From this observation, we designed gap models that incorporate small air gaps that will allow room for the bulging effect of each column of capacitors to fill and reduce the amount material between columns pressing against each other. We believe that the gap method will allow for increased longitudinal compression of the structure.

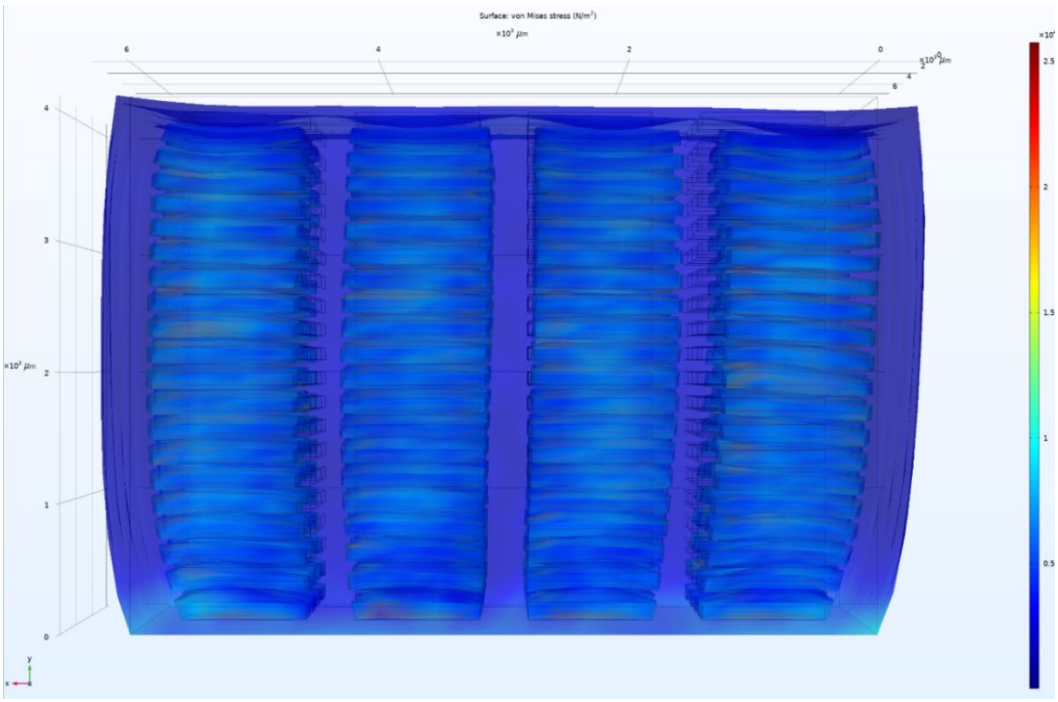

Figure 9. Force density heat map of 4x4x10 standard model COMSOL simulation.

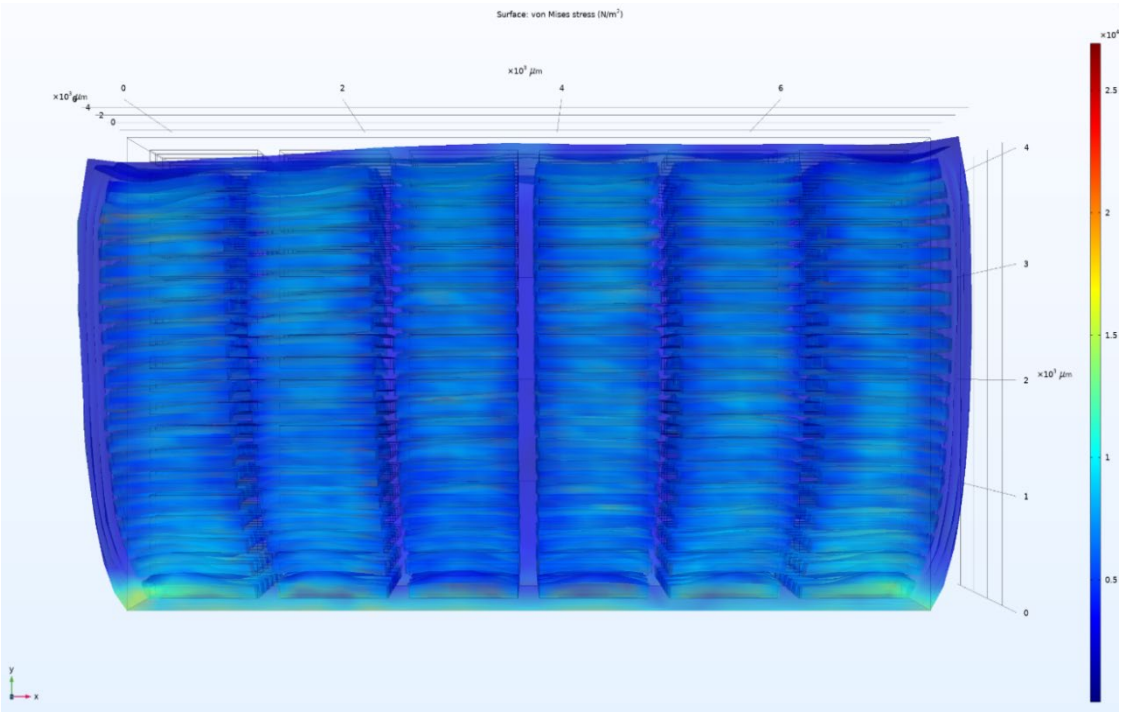

Figure 10. Force density heat map of 8x8x10 standard model COMSOL simulation.

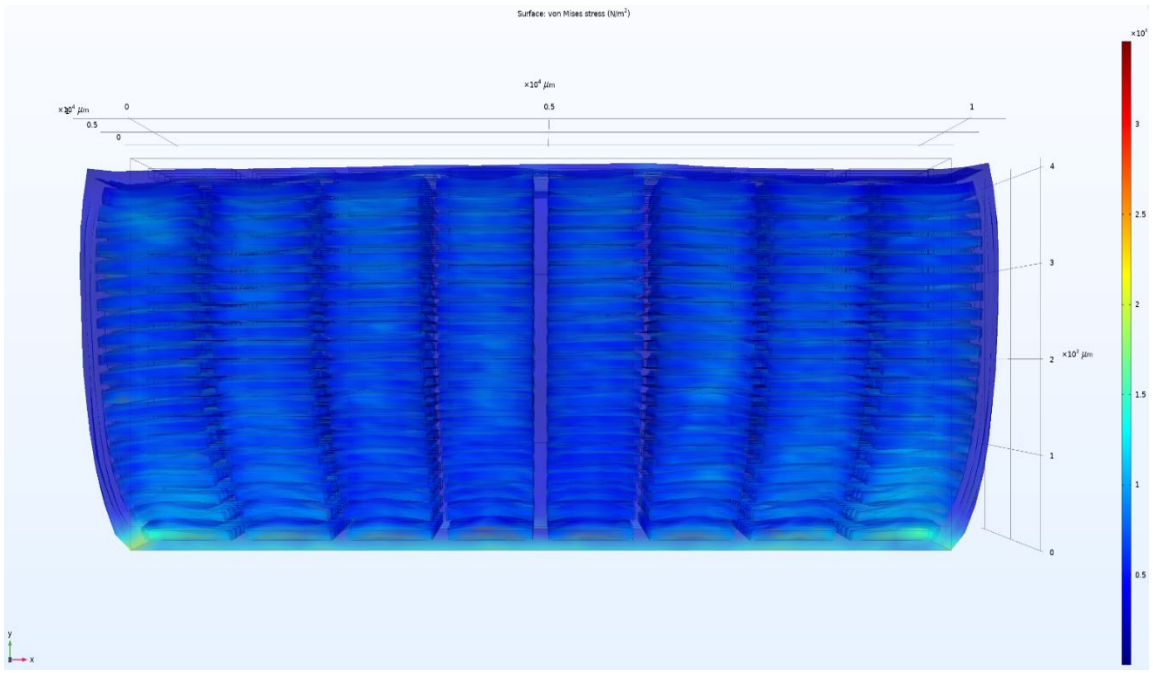

Figure 11. Force density heat map of 8x8x10 standard model COMSOL simulation.

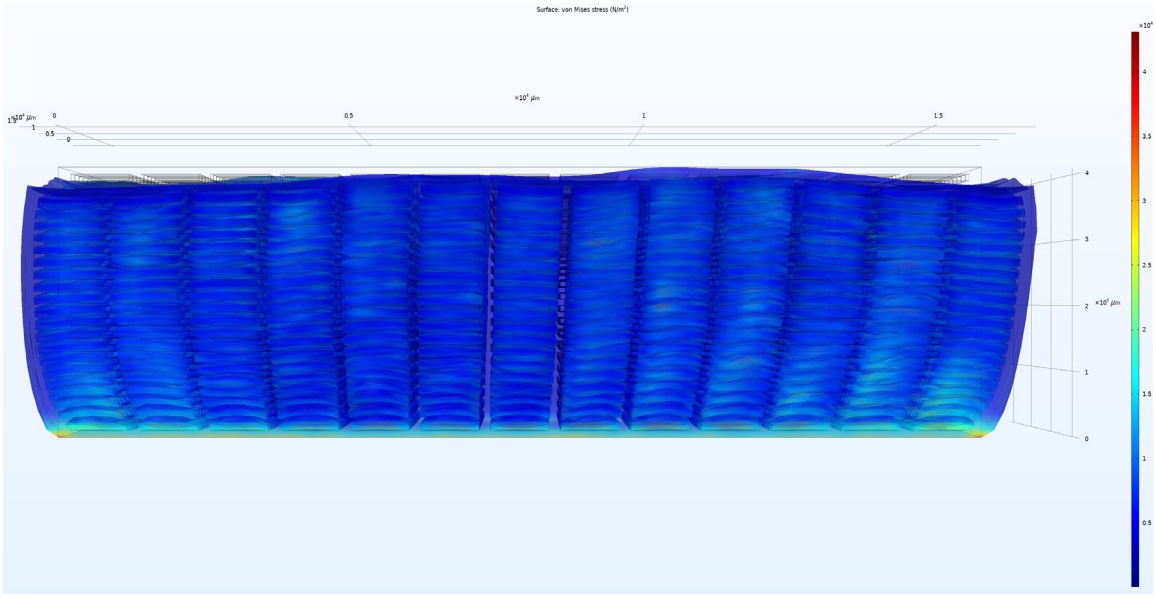

Figure 12. Force density heat map of 13x13x10 standard model COMSOL simulation.

After examining the results from the standard array and using that insight to design the gap array, we can answer thesis research question 3: An interactive visualization of a

three-dimensional virtual object is a suitable model for the human operator examination of the artificial muscle and optimization of its structure. As shown in Figures 13, 14, 15, and Table 6, a three-dimensional visual representation of the models conveyed enough information for the human user to understand how to optimize the models' parameters for a desired use, in our case, maximizing force density.

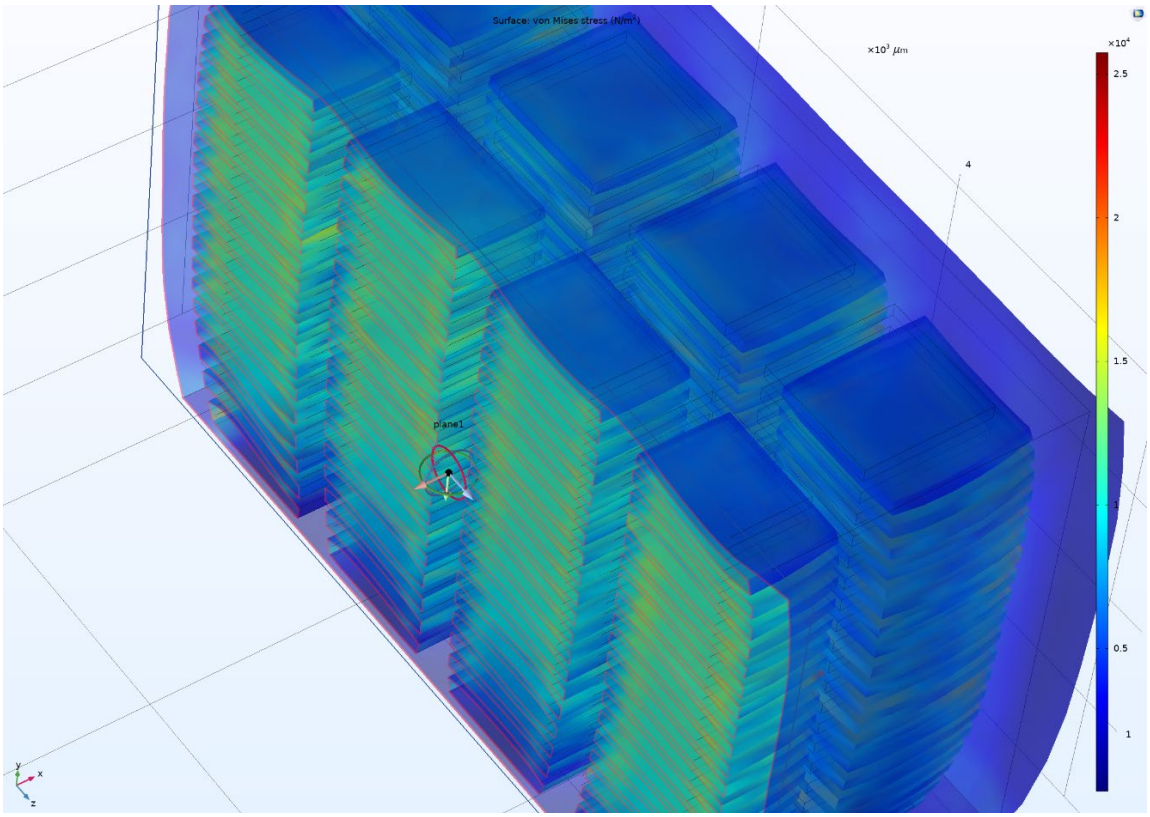

Figure 13. Force density heat map with plane slice for deformation evaluation of 4x4x10 standard array model.

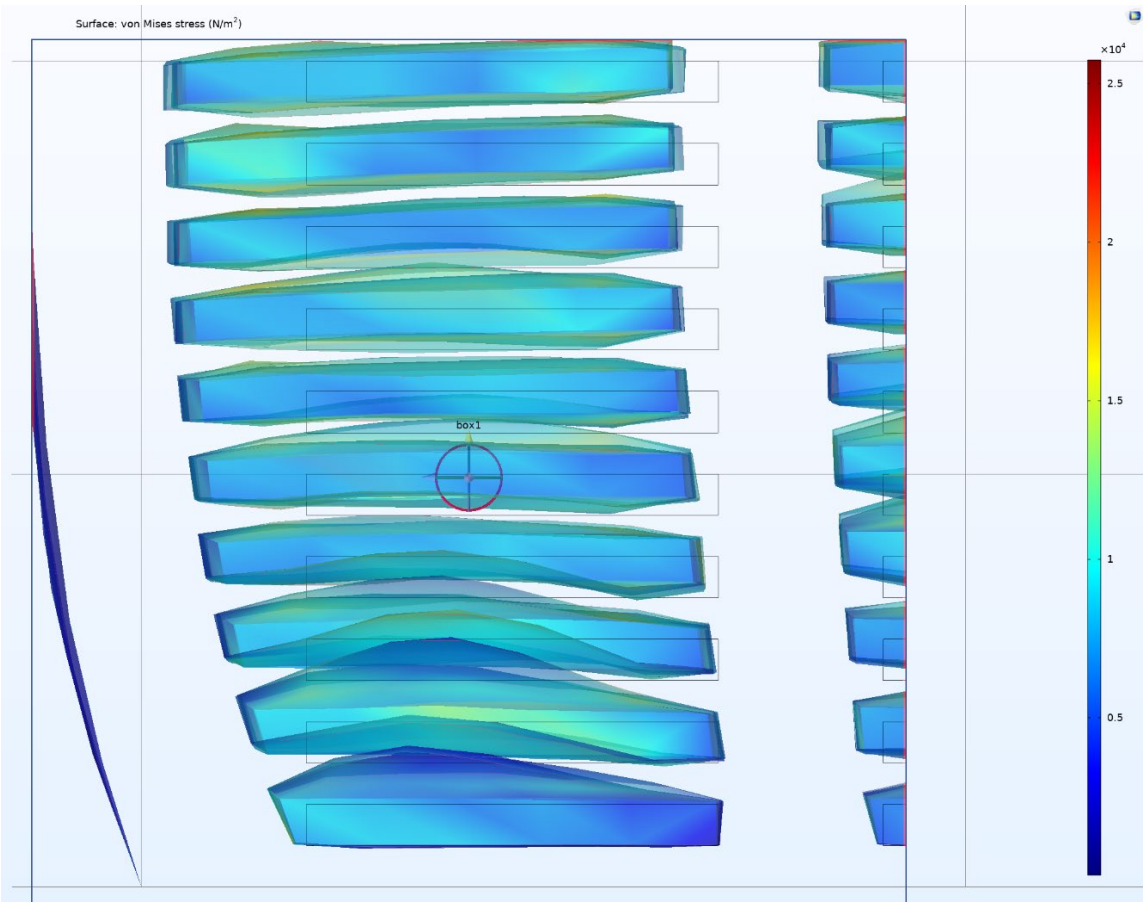

Figure 14. Force density heat map with box slice for deformation evaluation of 4x4x10 standard array model. Original location outlined in wireframe.

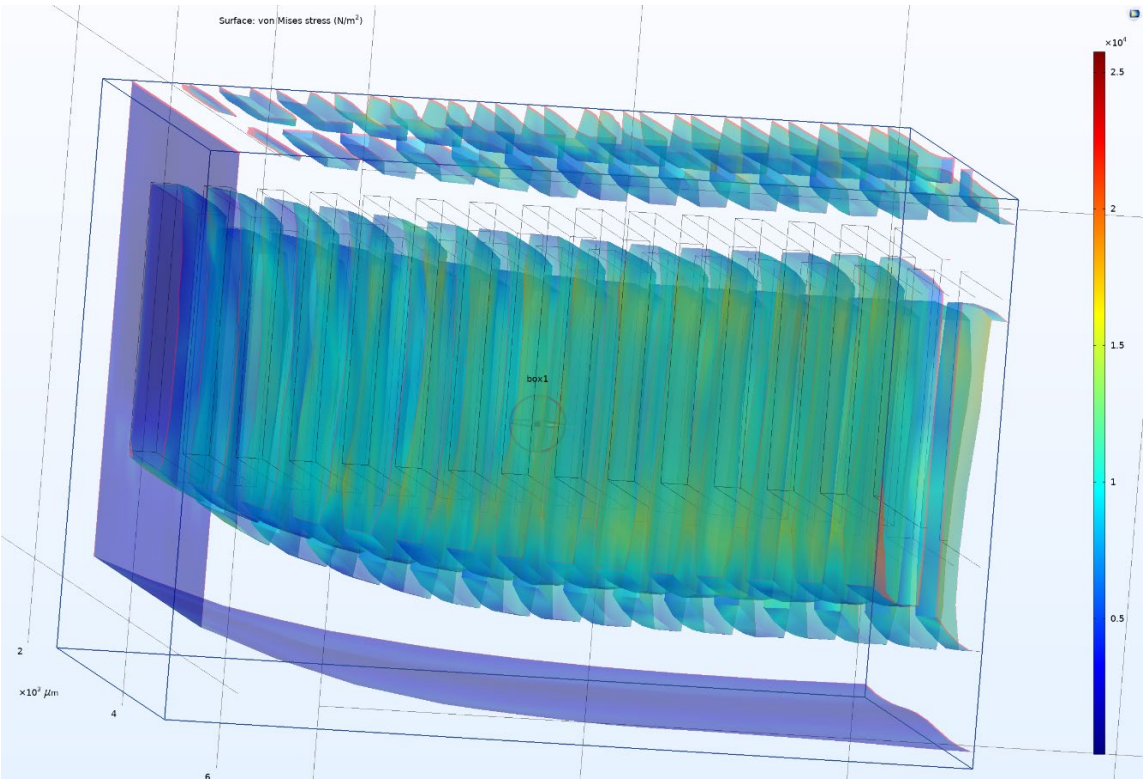

Figure 15. Force density heat map with box slice at angle for deformation evaluation of 4x4x10 standard array model. Non-deformed orientation outlined in wireframe.

At the conclusion of running all the standard arrays through the iterations of array sizes, we started evaluating the three-dimensional virtual object for ways to optimize the model and potently create a new model capable of creating more force. COMSOL allowed us to observe the interaction of forces both inside and outside the modeled artificial muscle. The primary reasons we did not utilize virtual reality for a more immersive and in-depth viewing and examination of the 3D standard array model was due to complexity, format, and fidelity. Once the simulation is completed, the resulting model is very complex with the small curves and boundaries that have been deformed due to the interacting forces. These details are observable only with COMSOL's suite of model manipulation tools that are paired to a mouse and keyboard user interface. The second and third reasons are the format and fidelity, both these reasons are inextricably linked so they will be outlined together. The model in its base form and undeformed is exportable in a format that other 3D processing programs can import and render in 3D. The mesh model after it has been

deformed, due to the stresses and strains induced by the COMSL software for our testing, cannot be exported in a format that can be visualized in a VR environment. We had hypothesized, before we were made aware that the format would not work, that the fidelity of the exported model would be high enough for proper evaluation in the VR environment it was displayed in, since the whole model would be imported as a single mesh and not as individual entities and boundaries for individual evaluation. This is why we chose to examine the 3D model on a desktop for optimization and not with a VR headset.

The COMSOL software outputs not only the stress, strain, and surface area we use to do the calculations for how strong the muscle is, but it also displays a high fidelity, highly accurate deformed model at the end of the simulation. The model can be sliced via an invisible plane, sphere, box or cylinder for internal viewing of internal deformed surfaces as shown in Figure 13, 14, and l5. The COMSOL software also has the post processing capability to display stress and strain gradients for easier visibility of the stress concentrations most apparent in Figure 14. The COMSOL software allows the user to manipulate the deformed model 360 degrees on all three axes. The user can also zoom in to view the deformed edges and entities as close as needed to accurately see the deformation on all boundaries also shown in Figure 13, 14, and l5.

B. EXPERIMENT 2, GAP METHOD

Analysis of standard array heat map and the above outlined reasons are why we want to explore a gap method model: As we can see from the heat map of the forces experienced by the standard array model, the structure bulges out laterally and appears to limit the amount that the structure can compress longitudinally. From this observation we will simulate a model that incorporates small air gaps that will allow room for the bulging effect of each column of capacitors to fill and reduce the amount material between columns pressing against each other. We believe that the gap method will allow for increased longitudinal compression of the structure at the expense of force density.

Analysis: Similar to the standard array models, the gap method models' max force density also increases along an asymptotic curve that saturates around 6750 Pa which is produced when simulating the 11x11x10 model. From the heat map of the forces

experienced by the structure shown in Figure 16 we can see that as the muscle contracts longitudinally, it simultaneously expands laterally. When comparing the standard models to the gap method models, we observe that the gap model does not expand more than the standard array, relatively speaking, however it does not produce a greater force density than the standard array even with the larger starting size due to the added gap geometry that had a saturation 8714.68 Pa which is produced when simulating the 12x12x10 model. When we compare the max force density for each array size from the standard array in Table 3 and the gap array max force densities in Table 4 the standard array produces more force at every array size than the gap array.

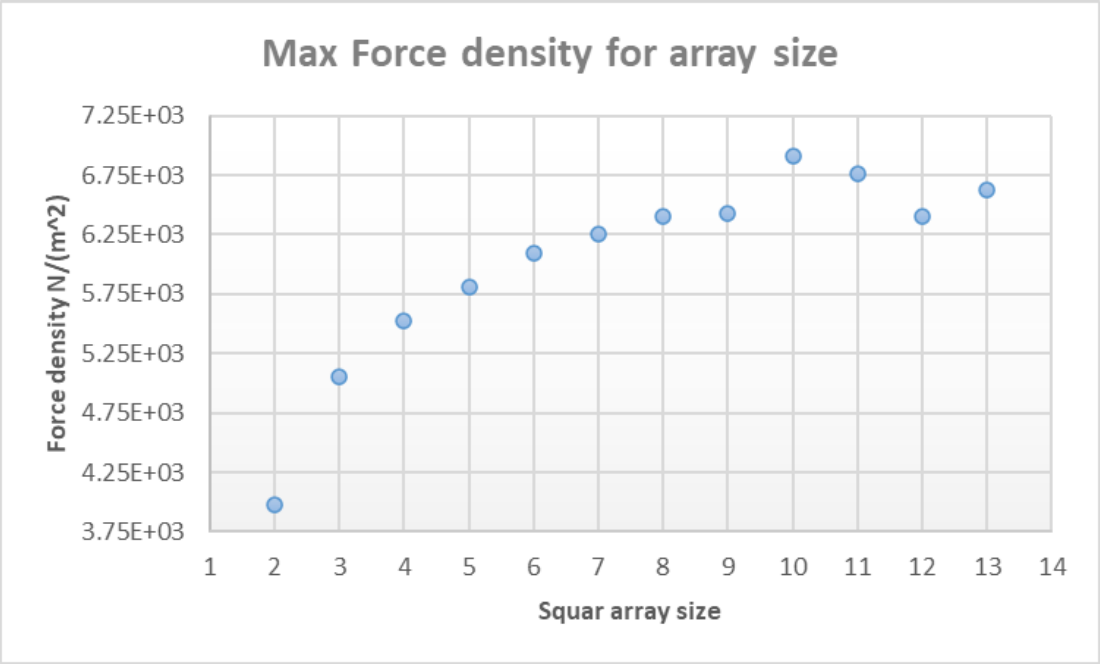

Figure 16. The max force density of n x n x 10 models where n equals 1 through 13.

Table 7. The max force density in pascals (Pa) and the corresponding u parameter that was used in the model.

Array Size	Max Force density, Pa	L param
2x2x10	3979.3083	100
3x3x10	5051.5271	110
4x4x10	5526.7254	110

5x5x10	5812.1206	110
6x6x10	6089.5978	110
7x7x10	6256.3889	110
8x8x10	6409.0909	110
9x9x10	6911.2475	110
10x10x10	8708.7806	100
11x11x10	6758.8174	100
12x12x10	6409.0909	110
13x13x10	6628.7039	100

We see from zoomed-in post simulation images of a 2x2 gap model, Figure 17 and Figure 18, how the air gaps allow for the latitudinal bulging to expand more uniformly without deforming the parallel columns of capacitors as much compared to the standard array. From this data we can answer thesis **research question 3**: The force density of planar polarity wired artificial muscle arrays with gap method converges on a single value around 6700 Pa or 0.97 PSI as the array is expanded longitudinally and laterally. From this data, we can also answer thesis **research question 4**: The optimal muscle-to-tendon ratio from the data gathered on the gap array simulations is approximately 75 to 25, which means that 75 percent of the surface area of the XY plane are microfluidic capacitors and 25 percent is the dielectric material and gaps. After examining the results from the gap method array in Table 7 and using insight gained from Figure 17–24 to produce innovative ideas for future research, we can confirm our answer to thesis **research question 5**: An interactive visualization of a three-dimensional virtual object is a suitable model for the human operator examination of the artificial muscle and optimization of its structure.

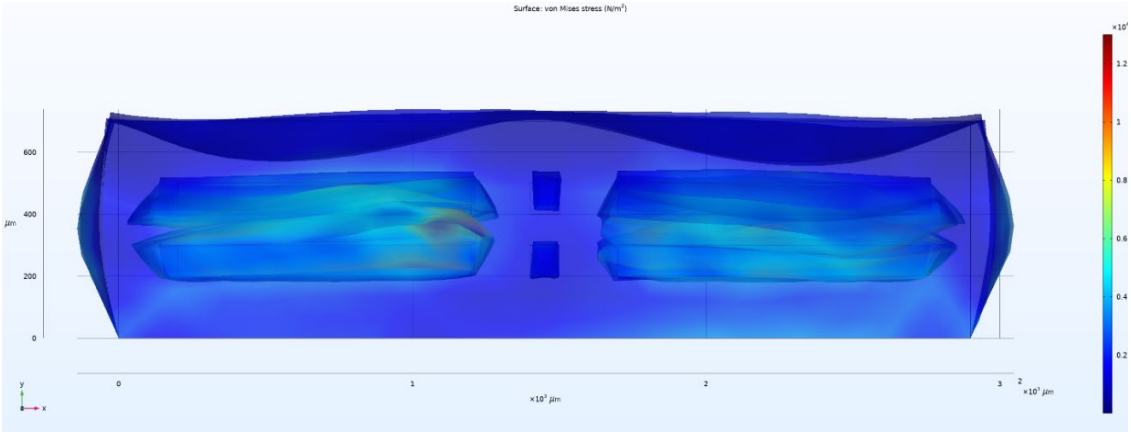

Figure 17. View from the XY plane of Von Mises stress induced by 3000 volts on a 2x2x1 array deformation of the microfluidic capacitors and deformation of the air gaps positioned longitudinally in the z plane.

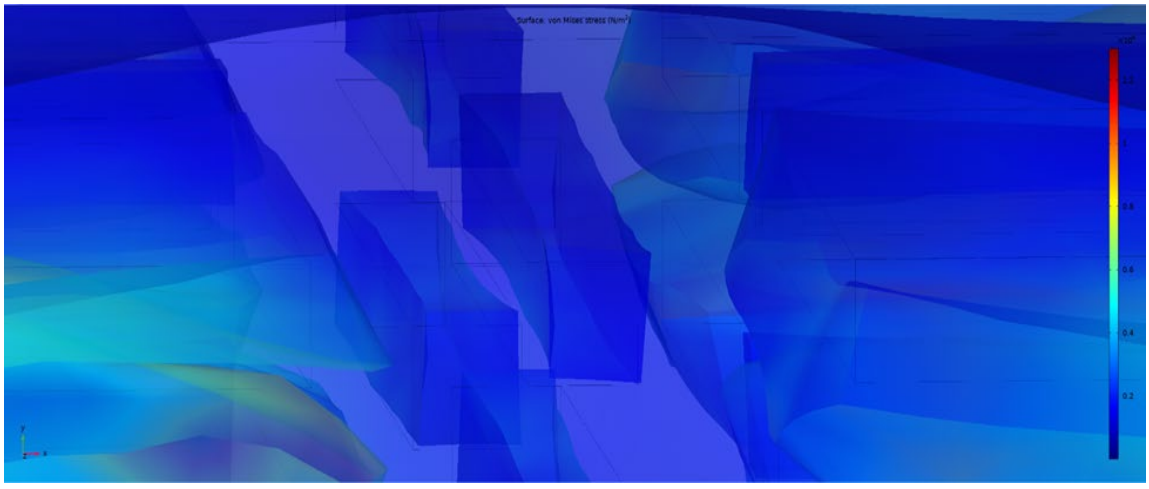

Figure 18. Close up view of the final deformation in the air gaps between the microfluidic capacitors with wire frame showing original orientation and location.

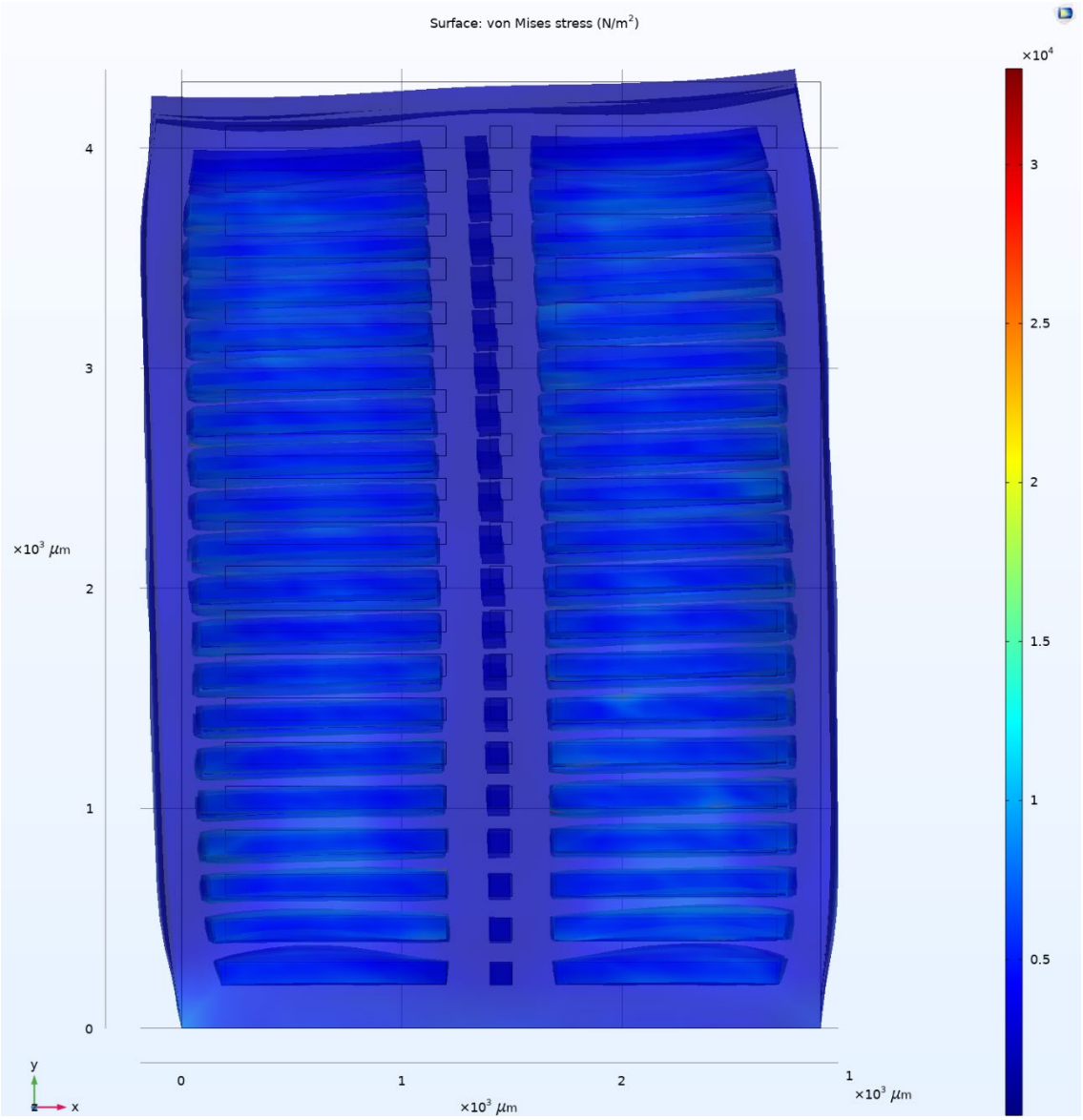

Figure 19. Force density heat map of 2x2x10 gap model COMSOL simulation.

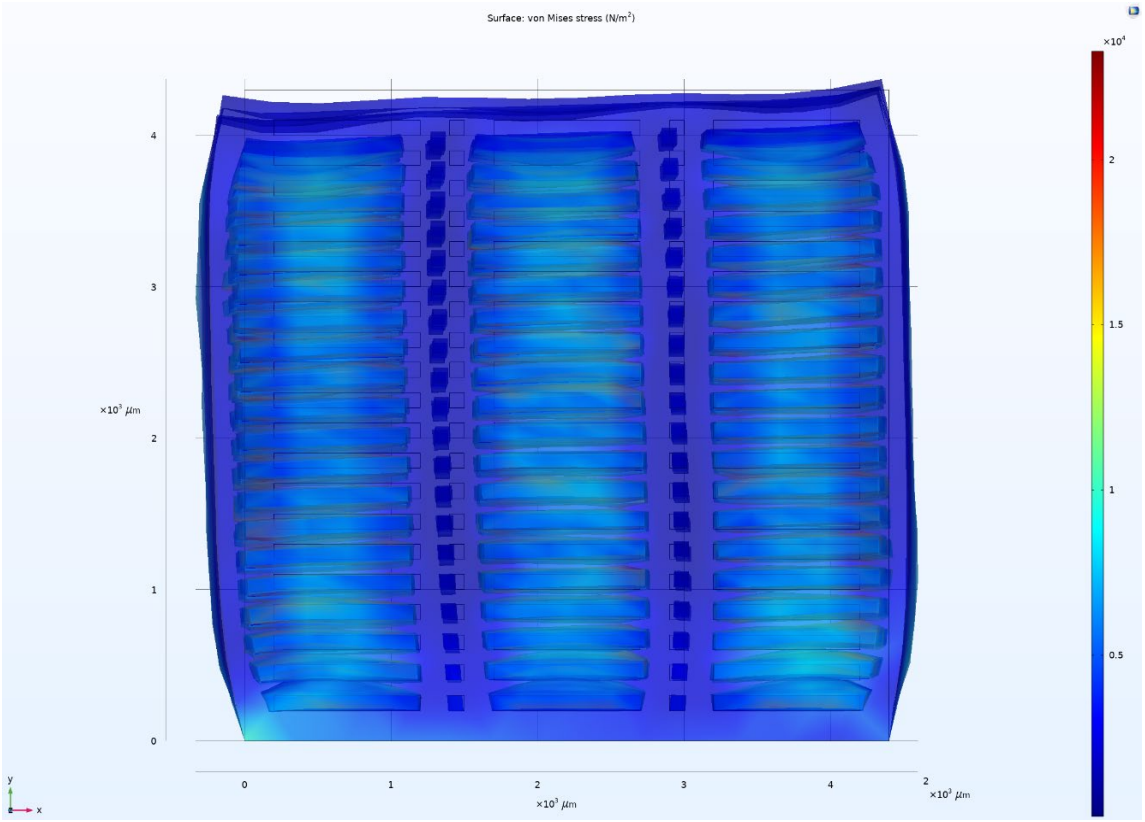

Figure 20. Force density heat map of 3x3x10 gap model COMSOL simulation.

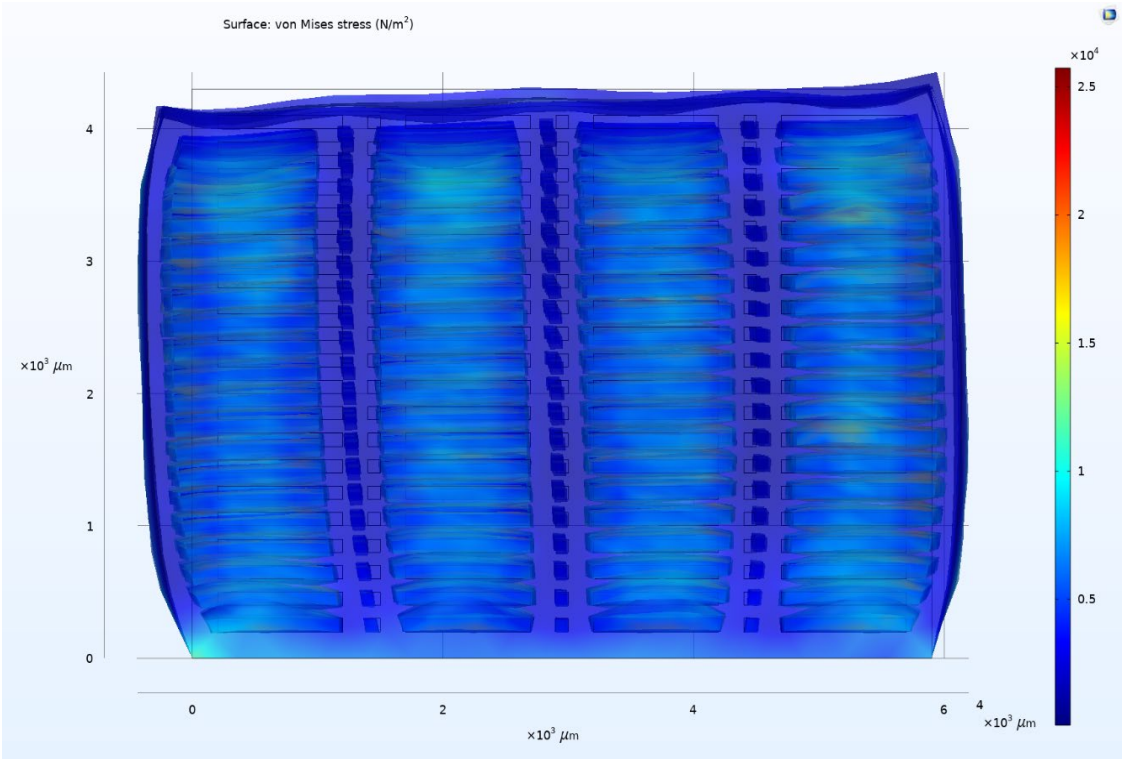

Figure 21. Force density heat map of 4x4x10 gap model COMSOL simulation.

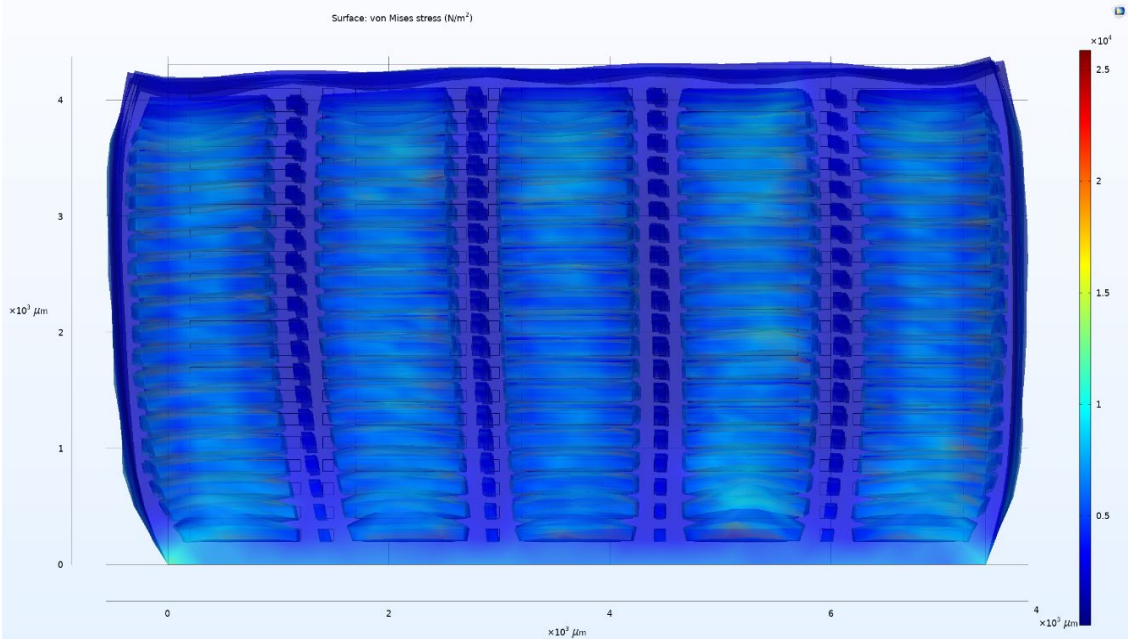

Figure 22. Force density heat map of 5x5x10 gap model COMSOL simulation.

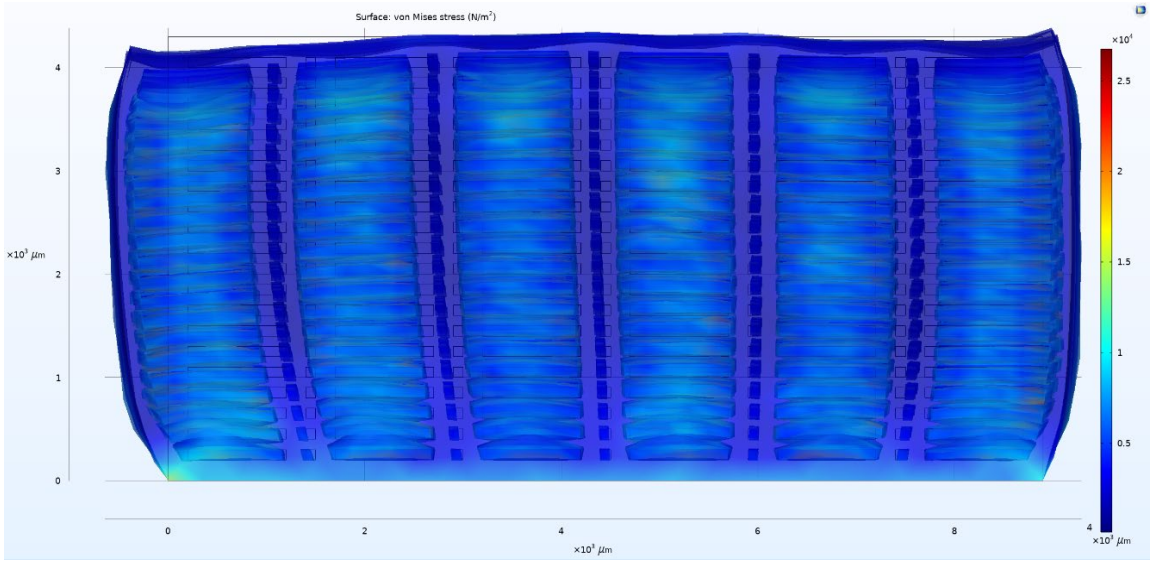

Figure 23. Force density heat map of 6x6x10 gap model COMSOL simulation.

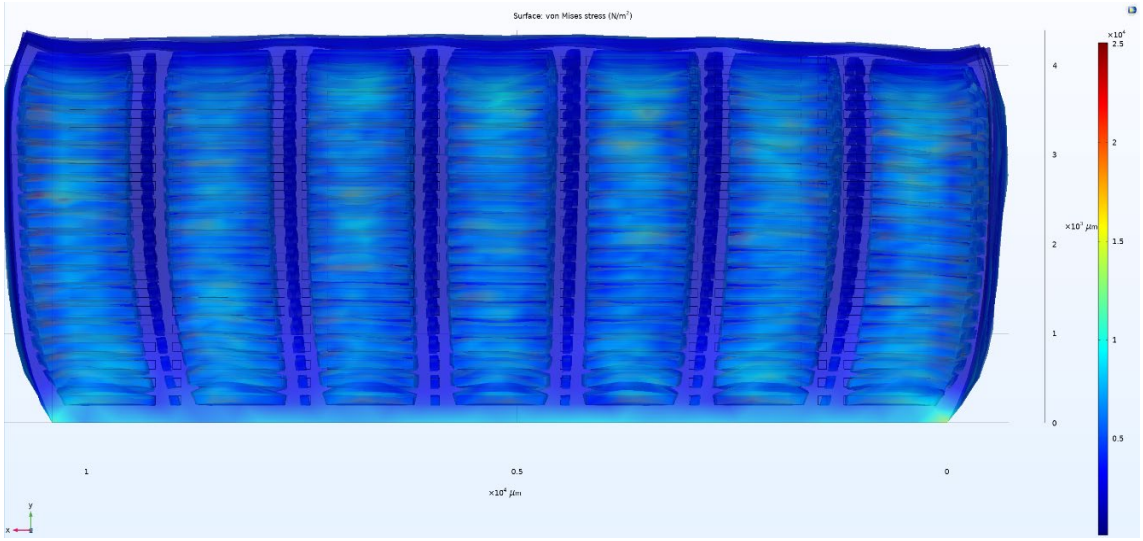

Figure 24. Force density heat map of 7x7x10 gap model COMSOL simulation.

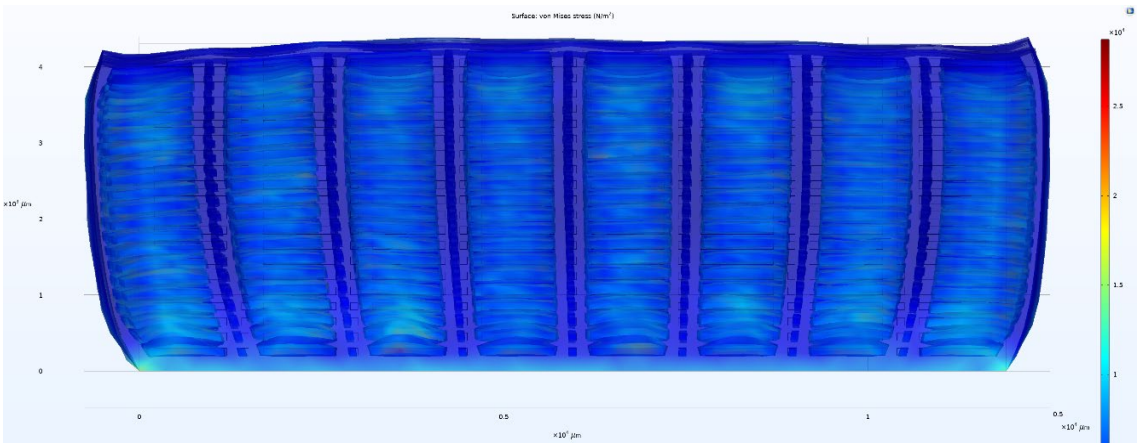

Figure 25. Force density heat map of 8x8x10 gap model COMSOL simulation.

C. CHAPTER SUMMARY

In this chapter we presented the values obtained from both the standard array and the gap array and plotted both array values on graphs for comparison. We also presented all relevant data sets and addressed each research question.

THIS PAGE INTENTIONALLY LEFT BLANK

VI. CONCLUSIONS AND RECOMMENDATIONS

A. MAIN CONCLUSIONS AND RECOMMENDATIONS

We conducted COMSOL simulations of electrostatically-actuated artificial muscles for the standard array based on microcapacitor arrays of size NxNx10, where N is between 1 and 13. For each simulated array, tendon thickness, or dielectric material between microfluidic capacitors, the parameter was incremented to determine maximal output force density, which was then plotted against the arrays size. The resulting curve saturated at N=10 and force density of ~8800 Pa, with an optimal muscle-to-tendon ratio of 9 to 1. COMSOL simulations of a 10x10x10 standard array is sufficient to predict the behavior of macroscopic artificial muscles with microcapacitors configured in the same way, thus allowing for important analyses to be achieved rapidly with relatively modest computational resources. Furthermore, the shown saturation force density of ~8800 Pa at 100 μm scale of the standard array constituent devices can now be used to predict the performance of practical standard array macroscopic actuators. The optimal muscle-to-tendon ratio from the data gathered on the standard array simulations is approximately 9 to 1, which means that 90 percent of the surface area of the XY plane are microfluidic capacitors, and 10 percent is dielectric material as shown in Table 6. The shown saturation force density of ~6700 Pa at 100 μm scale of the gap array constituent devices can now be used to predict the performance of gap array macroscopic actuators. The optimal muscle-to-tendon ratio from the data gathered on the gap array simulations is approximately 75 to 25, which means that 75 percent of the surface area of the XY plane are microfluidic capacitors and 25 percent is the dielectric material and gaps as shown in Table 7. Both achieved conclusions contribute to reducing the cost of developing and designing artificial muscles as well as providing a benchmark force density output for future work to be compared to as a baseline. Furthermore, we can conclude that COMSOL generated three-dimensional virtual objects are a suitable model for the human operator to examine the artificial muscle models and optimization its structure as we did when we manipulated the post simulation force distribution models to design the gap array.

B. THESIS CONTRIBUTIONS

The main contribution to the artificial muscle domain is a successfully simulated baseline ratio of muscle that can generate force and transfers the force of an electrostatically actuated artificial muscles based on microcapacitor arrays. The ratio found for this method has a very high stress that induces a force transferring ratio for the allotted space that a muscle could take up in each scenario or muscle setup. The ideal tendon thickness as determined in the simulation for a standard array allows for the expansion of study into other areas of the muscle for experimentation. Upon the verification and validation of the simulated values from a 3D-printed prototype, specific applications and simulations can be started to determine the optimal real-world application of this type of artificial muscle. Ideally, different geometries and layouts may prove to be more effective at the efficient transfer of forces through the muscle and tendon arrays.

C. FUTURE WORK

With the COMSOL simulation producing viable results for electrostatically actuated artificial muscles based on micro fluidic capacitor arrays, there are numerous research and experimentation directions to expand on by future researchers. We recommend expanding the size of the simulations in COMSOL used to determine the ideal gap width to allow for further contraction of the overall structure when the microcapacitors are under full voltage load. The geometry of the gap is also a future research topic of interest as it pertains to the level of strength and contraction that can be built into the tendon areas inside the muscle arrays. The shape of the gap will also play a part in the way that muscle is flexed and the way that flex manifests itself in the desired motion of the item the muscle is actuating. For example, if the muscle is being used in biomimetic underwater propulsion, that muscle must not only transmit load but flex with the movement of the robot fish it is propelling. It stands to reason that the shape of the gap inside the muscles will be crucial in allowing the muscle to be both flexible and strong in the desired orientation. Several lines of future work stem from the results, their implications and areas we did not have the time to explore.

1. Microcapacitor Configurations

One of the areas we did not have time to explore was for COMSOL to include simulation of different microcapacitor configurations. Such as expanded research and experimentation of the standard array into more organic type geometry and run COMSOL simulations with different shapes of the micro fluidic capacitors and different shapes of the tendons to determine if more efficient designs can be derived from further application and study of biomimetics. Similar to the idea of the gap method, future simulations will bring insight and innovative ideas of how to build more efficient artificial muscles.

2. Verification and Validation

An area we worked on outside the thesis process, but ultimately did not achieve, was to 3D printing artificial muscles to the optimal parameters found in our study and then conducting real tests of the force outputs. The primary starting point for testing and 3D printing the existing designs will be to print the standard array design and compare the derived results from COMSOL to those obtained from a 3D-printed prototype. Through this process of verifying and validating the methodology of electrostatically actuated microcapacitor arrays of real and fully manufactured artificial muscles the COMSOL models can continue to be used for development as the ratio of modeled to actual force can be documented. The same process would be accomplished for the gap array method, the force output from the COMSOL model will be compared to the force outputs achieved from the printed prototype. It is noted that the resulting difference from the simulated standard array and the printed standard array to the simulated gap array and the printed gap array could be substantially different as we have introduced air pockets into the gap model and how an incompressible gas plays a role in the 3D-printed model is not yet verified.

3. 3D-Printed Muscle Durability

An interesting topic brough up by our study of 3D-printed materials was durability. Studies will need to be conducted into the efficiency and durability that these types of 3D-printed muscles can sustain. While the general material properties of the simulated generic dielectric material in COMSOL ware suitable for the purpose of a successful simulation,

the advancements in material science in the area of dielectrics that behave in ways that would benefit the area of artificial muscle are expanding. The task of developing and testing a dielectric with the ideal properties of high load cycle deterioration resistance, high voltage breaching resistance, and low deformation memory, to name a few, will be challenging as this material must be able to be 3D printed. Keeping in mind the manufacturability to maintain the modularity of this type of artificial muscle is quite a tall order for a researcher in the material science realm. Manufacturability will highly impact the efficiency, quality, and output of this artificial muscle in the areas of acoustic translucent underwater propulsion and exoskeletal locomotion.

4. 3D-Printed Muscle Impacts of Temperature

Another area of future research that plays a huge part in the material science of the dielectric part of the muscle is the effects of temperature on both the dielectric and more critically the liquid inside the electrostatically actuated microfluidic capacitors. For the sake of modeling simplicity in the COMSOL simulations, water was used for both the positive and ground sides of the microfluidic capacitors. Water properties are susceptible to temperature change and how it interacts with the semi-elastic dielectric as the operating temperature changes is an area where there is a great amount of research to be done. The fluid inside the microfluidic capacitors and the semi-elastic dielectric should be optimized for the gamut of temperatures in potential operating environments to include the cycling of temperatures in that environment. A combination of the optimization of the dialectic with respect to temperature and repeated loading patterns will be the cycling speed of the muscle or how fast it can go from at-rest position to fully flexed and back again. While initial estimates are promising for a quick response rate and cycle time, further research into the optimal dielectric compression coefficient with respect to temperature will heavily impact the cycle time and how fast the muscle can return to its unflexed position. For example, these challenges will heavily impact the usability of this design in translucent underwater propulsion in areas where the muscle will be subject to extreme water temperatures and then brought back aboard the ship to room temperature.

5. Electrostatic Optimization

The final area of the future research is in a similar vein as the last one: it involves the microfluidic capacitor and specifically the level of voltage loss at either full load or simple residual voltage bleed either via a catastrophic loss in the breaching of the dielectric material or in low level loss in the resistance of the liquid itself. The optimizing of the electrostatic portion of this microcapacitor arrays is a broad area of research and development for making the system safer and more efficient as loss of power plagues all systems and minimizing loss will be crucial to maximizing the performance of the system.

D. CONCLUSION

The effects of a 3D-printed, fully scalable, electrostatically actuated artificial muscles based on microcapacitor arrays on the USN/USMC/USA/DOD could be entirely game changing as theoretically once the muscle has been flexed via the application of voltage to induce electrostatic load the muscle will maintain its flexed status after the voltage is shut off. An artificial muscle capable of this type of actuation will be a great improvement over the current artificial muscle available in industry.

The gap simulations are very promising, but we find it surprising that at the same device size, the max output force density is lower than the one in the same-size standard array. Our guess is it may have to do with the horizontal posts between the muscle fibers, however, more research needs to be invested to identify the true cause. To illustrate it, one can consider the space between adjacent fibers as capital H, where the lines are dielectric. The H has a gap above and a gap below the horizontal central bar. That bar may be the problem. It provides some structural strength, but our best guess based on what we know about this domain is that it also significantly limits the ability of the fibers to expand laterally. That expansion is what we want to maximize and take advantage of the gap effect and non-linearity of the force.

THIS PAGE INTENTIONALLY LEFT BLANK

APPENDIX A. LINUX CODE

Linux code required to run a COMSOL simulation on the Naval Postgraduate Schools High Performance Computing system called "Hamming," this code was provided by Dr. Paul Leary as a nano file to run specific COMSOL simulation files on the supercomputer.

```
#!/bin/bash
#######################################
#SBATCH --job-name=comsol_test  # Name of job
#SBATCH --nodes=4               # Number of nodes
#SBATCH --cpus-per-task=64      # Number of cores per node
#SBATCH --mem=0                 # Request all available memory
#SBATCH --time=4-13:00:00       # Syntax is DD-HH:MM:SS
#SBATCH --output=output-%j.txt  # Name of output file
#SBATCH --hint=nomultithread    # turn off multi-threading
##SBATCH --reservation=comsol    # uncomment if we have a reservation
#######################################
. /etc/profile
module load compile/intel
module use /share/modules/restricted/app
module load comsol
comsol batch -mpibootstrap slurm -nn ${SLURM_NNODES} -np ${SLURM_CPUS_PER_TASK} -inputfile "filename" -outputfile "filename"
```

THIS PAGE INTENTIONALLY LEFT BLANK

LIST OF REFERENCES

[1] T. McKenna, "Bio-inspired autonomous systems," Office of Naval Research, April 25, 2021. [Online]. Available: https://www.onr.navy.mil/en/Science-Technology/Departments/Code-34/All-Programs/human-bioengineered-systems-341/bio-inspired-autonomous-systems

[2] M. A. Coltelli, J. Catterlin, A. Scherer, and E. P. Kartalov, "Simulations of 3D-printable biomimetic artificial muscles based on microfluidic microcapacitors for exoskeletal actuation and stealthy underwater propulsion," *Sensors and Actuators. A. Physical.*, vol. 325, p. 112700–, 2021. [Online]. Available: https://doi.org/10.1016/j.sna.2021.112700

[3] G. Dybicz, email, Stratasys associate process manufacturing engineer, Apr. 2021.

[4] B. Kalita and S. K. Dwivedy, "Dynamic analysis of pneumatic artificial muscle (PAM) actuator for rehabilitation with principal parametric resonance condition," *Nonlinear Dynamics*, vol. 97, no. 4, pp. 2271–2289, Sep. 2019, Available: [Online]. Available: https://doi.org/10.1007/s11071-019-05122-2

[5] R. E. Pelrine, J. S. Eckerle, and S. Chiba, "Review of artificial muscle approaches," *In An Invited Paper, in Proc. Third Int. Sym. on Micro. Mach. and Hum. Sci.*, Nagoya, Japan, 1992. Available: [Online]. Available: https://www.researchgate.net/publication/354343098

[6] J. Paquette and K. Kim, "Ionomeric electroactive polymer artificial muscle for naval applications," *IEEE Journal of Oceanic Engineering*, vol. 29, no. 3, pp. 729–737, 2004. [Online]. Available: https://doi.org/10.1109/JOE.2004.833132.

[7] H. Song and Y. Hori, "Force control of twisted and coiled polymer actuators via active control of electrical heating and forced convective liquid cooling," *Advanced Robotics*, vol. 32, no. 14, pp. 736–749, Jul. 2018, [Online]. Available: https://doi.org/10.1080/01691864.2018.1494629.

[8] P-J. Cottinet, D. Guyomar, J. Galineau, and G. Sebald, "Electro-thermo-elastomers for artificial muscles," *Sensors and Actuators. A. Physical*., vol. 180, pp. 105–112, 2012. [Online]. Available: https://doi.org/10.1016/j.sna.2012.04.016.

[9] N. D. Naclerio and E. W. Hawkes, "Simple, low-hysteresis, foldable, fabric pneumatic artificial muscle," in *IEEE Robotics and Automation Letters*, vol. 5, no. 2, pp. 3406–3413, April 2020. [Online]. Available: https://doi.org/10.1109/LRA.2020.2976309.

[10] B. G. Liptak, *Instrument Engineers' Handbook: Process Measurement And Analysis*, vol. II. Boca Raton, FL, USA, CRC Press, 2004.

[11] H. Al-Fahaam, S. Davis, and S. Nefti-Meziani, “The design and mathematical modelling of novel extensor bending pneumatic artificial muscles (EBPAMs) for soft exoskeletons,” *Robotics and Autonomous Systems*, vol. 99, pp. 63–74, 2018. [Online]. Available: https://doi.org/10.1016/j.robot.2017.10.010.

[12] C. Qi, F. Gao, H.-X. Li, S. Li, X. Zhao, and Y. Dong, “An incremental Hammerstein-like modeling approach for the decoupled creep, vibration and hysteresis dynamics of piezoelectric actuator,” *Nonlinear Dynamics*, vol. 82, no. 4, pp. 2097–2118, Dec. 2015. [Online]. Available: https://doi.org/10.1007/s11071-015-2302-z.

[13] W.-S. Chu et al., “Hybrid manufacturing in micro/nano scale: A Review,” *International Journal of Precision Engineering and Manufacturing - Green Technology*, vol. 1, no. 1, pp. 75–92, 2014. [Online]. Available: https://doi.org/10.1007/s40684-014-0012-5.

[14] T. Higuchi, K. Suzumori, and S. Tadokoro, *Next-Generation Actuators Leading Breakthroughs*, London: Springer London, 2010. [Online]. Available: https://doi.org/10.1007/978-1-84882-991-6.

[15] J. Ru et al., “Controllable and durable ionic electroactive polymer actuator based on nano porous carbon nanotube film electrode,” *Smart Materials and Structures*, vol. 28, no. 8, p. 85032–, 2019. [Online]. Available: https://doi.org/10.1088/1361-665X/ab2a28.

[16] H. Liu et al., “An electrically actuated soft artificial muscle based on a high-performance flexible electrothermal film and liquid-crystal elastomer,” *ACS Applied Materials & Interfaces*, vol. 12, no. 50, pp. 56338–56349, 2020. [Online]. Available: https://doi.org/10.1021/acsami.0c17327.

[17] J. Szkopek, G. Redlarski, and A. Zak, “Electrostatic zipping actuators-analysis of the pull-in effect depending on the geometry parameters,” *Energies (Basel)*, vol. 14, no. 24, p. 8355–, 2021. [Online]. Available: https://doi.org/10.3390/en14248355.

[18] J. Zhang et al., “Robotic artificial muscles: current progress and future perspectives,” *IEEE Transactions on Robotics*, vol. 35, no. 3, pp. 1–21, 2019. [Online]. Available: https://doi.org/10.1109/TRO.2019.2894371.

[19] H. S. Cho, T. H. Kim, T. H. Hong, and Y.-L. Park, “Ratchet-integrated pneumatic actuator (RIPA): a large-stroke soft linear actuator inspired by sarcomere muscle contraction,” *Bioinspiration & Biomimetics*, vol. 15, no. 3, pp. 036011–036011, 2020. [Online]. Available: https://doi.org/10.1088/1748-3190/ab7762.

[20] *Additive manufacturing policy*, MCO 4700.4, Department of the Navy, Washington, DC, USA, 2020 Available: [Online]. Available: https://www.marines.mil/News/Publications/MCPEL/Electronic-Library-Display/Article/2147107/mco-47004/

[21] P. Rothemund, N. Kellaris, S. K. Mitchell, E. Acome, and C. Keplinger, “HASEL artificial muscles for a new generation of lifelike robots—recent progress and future opportunities,” *Advanced Materials (Weinheim)*, vol. 33, no. 19, p. e2003375–n/a, 2021. [Online]. Available: https://doi.org/10.1002/adma.202003375.

THIS PAGE INTENTIONALLY LEFT BLANK

INITIAL DISTRIBUTION LIST

1. Defense Technical Information Center
   Ft. Belvoir, Virginia

2. Dudley Knox Library
   Naval Postgraduate School
   Monterey, California